Solid State Research

Lincoln Laboratory

MASSACHUSETTS INSTITUTE OF TECHNOLOGY

Division 8

Group 53

Group 26

1961

No. 4

Issued 14 March 1962

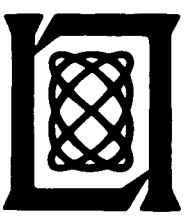

INTRODUCTION

I. SOLID STATE DEVICE DESIGN

The photoconductivity and absorption cross section of antimony-compensated copper-doped Ge are being studied as a function of wavelength. These measurements on samples in which Cu^{--} states were partially full ($2N_{Cu} > N_{Sb} > N_{Cu}$) have indicated, in agreement with thermal activation energies measurements, that the Cu^{--} energy level is located 0.32 ev above the valence band. The shapes of the curves also have indicate that this level does not have a discrete $\vec{k}$ value. Several samples in which the Cu^{---} levels were partially full ($3N_{Cu} > N_{Sb} > 2N_{Cu}$) have shown an anomalous decrease in absorption at 0.26 ev while from the photoconductivity data and thermal activation measurements one would expect an increase in absorption.

A large negative resistance region has been observed in the forward characteristics at 77°K of n^+p InSb diodes in which the thickness of the p-base is large (>1 mm) compared with the minority carrier diffusion length. Experimental units have been switched from their high-impedance state to their low-impedance state or vice versa in times of the order of 10^{-7} seconds. Experiments have shown that this negative resistance is produced by conductivity modulation of the base region, which is greatly enhanced by a large increase in minority carrier lifetime when the minority carrier traps are saturated. The I-V characteristic of this negative resistance diode is extremely sensitive to magnetic field perpendicular to the direction of current flow in the base region. In preliminary devices, the diode current has been changed by more than 50 ma by an application of less than 5 gauss (~4 amp-turns/cm). The effect of the magnetic field is to decrease the minority carrier diffusion length and the conductivity modulation of the base region. Measurements of the Suhl-effect indicate that most of the change in diffusion length is due to a change in effective lifetime. Very preliminary measurements on "thick-base" InSb n^+pn transistors have shown extremely large effects of magnetic fields on the current gain.

Fabrication techniques have been developed for PbSe tunnel diodes. Diode evaluation has been helped by the construction of a conductivity plotter. Deposition rate and surface finish of epitaxial germanium layers are under good control, and efforts are now directed toward producing layers of uniform and reproducible resistivity.

II. CHEMISTRY

Concluding experiments dealing with co-conduction by solutions contacting germanium provide further substantiation of a general theory of co-conduction. A stable electron-limited current was found for a p-type germanium electrode at several solution compositions, for which the cathodic reaction evidently consumes conduction band electrons.

A correlation between thermal etch pits and edge dislocations was found for germanium {111} surfaces. Thermal etch rates have been measured for the principal low-index planes.

Measurements of the spontaneous bending of very thin InSb single crystals have been quantitatively interpreted in terms of the strain associated with the distortion of the In {111} surface bonds.

Measurements of the Seebeck coefficient, resistance and magnetic susceptibility of PrO_x single crystals are continuing. Measurements of the Seebeck coefficient and resistance of SnO_2 single crystals have been initiated; temperature regions of intrinsic and extrinsic conduction have been observed.

A table of mass spectrographic lines has been compiled for RF spark ionization of inorganic solids in a Mattauch-Herzog double-focusing mass spectrograph. Use of a tapered capillary is being investigated for eliminating effects of surface-active organic contaminants in the polarographic analysis of Hg-Cd-Te.

III. MATERIALS RESEARCH

The stoichiometry of $Cd_xHg_{1-x}Te$ alloys is being investigated by measuring the Hall coefficients of samples annealed in evacuated ampoules or in the presence of mercury vapor. Since a number of low-cadmium samples are in the mixed conduction range even at 4.2°K, an overlapping band model seems to apply to these alloys and to HgTe.

An apparatus has been constructed for determining superconducting transition temperatures by making continuous measurements of relative permeability as a function of temperature. The transition temperatures of $NbSb_xSn_{1-x}$ alloys have been found to decrease monotonically as x increases. The superconducting compound Nb_3In (transition temperature 9.2°K) has been synthesized for the first time, by the application of high pressure.

We are investigating the possibility of obtaining large crystals of Ge or Si uniformly doped with S, Se, or Te by using the Group VI elements as carriers for vapor-phase growth. Preliminary results have been favorable.

The lowest oxide of praseodymium that has been reported previously is $PrO_{1.5}$. An oxide of slightly lower valency, $PrO_{1.47}$, has been prepared, and its structure has been determined.

In a program on the growth of metal whiskers, iron whiskers up to 20 mm long and chromium whiskers up to 3 mm long have been prepared.

Hysteresis has been observed in the polymorphic transformation of various selenides under high pressure. The high-pressure phase of HgSe has been retained at atmospheric pressure by cooling the compressed samples below room temperature. The polymorphic transformation recently reported for InSb has been confirmed.

IV. BAND STRUCTURE OF SOLIDS

The measurements of optical absorption carried out on compensated and uncompensated donors in sulfur-doped silicon have been extended and interpreted in terms of a simple effective mass theory. Cyclotron resonance measurements have been made of the location and curvature of the third valence band in p-type diamond and also of the curvature of degenerate heavy hole bands.

Considerable effort has been devoted to the calculation of such transport properties as galvanomagnetic and galvano-thermomagnetic effects, Landau levels and resonance phenomena. Galvanomagnetic effects in n-type germanium are being studied as a function of scattering. The galvanothermomagnetic theory is being carried out for nonparabolic energy bands in degenerate materials as a function of the scattering processes. The study of the motion of Bloch electrons in a magnetic field for different types of orbits is being continued. By using a general statistical mechanical theory, the magnetic and cyclotron resonance phenomena have been derived theoretically.

V. MICROWAVE AND MAGNETIC PROPERTIES OF SOLIDS

As a further step in investigating various antiferromagnetic materials at millimeter wavelengths, a new method has been explored which utilizes powdered samples rather than single crystals. It has

been demonstrated by an analysis and comparison of data from single crystal and powdered $MnTiO_3$ that useful information can be obtained from powdered materials. This will help alleviate the difficulty of growing single crystals of sufficient purity to obtain significant data, since small amounts of impurities frequently alter the internal fields markedly.

The temperature dependence of the internal fields in Cr_2O_3 has been measured, independent of knowledge of the ratio of the parallel-to-perpendicular susceptibilities, by taking the resonance data with the applied field perpendicular to the c-axis.

Further measurements and analyses have been made of quantum effects in cyclotron resonance at 2 mm in silicon and germanium. In general, the theory provides an excellent fit to the experimental data.

Several natural crystals have been investigated by paramagnetic resonance techniques at 1-cm and 4-mm wavelengths for suitability as millimeter maser materials. One of the crystals, Al_2SiO_5, satisfies the preliminary requirements by virtue of the zero-field splittings and relaxation times.

Further experiments have been carried out in which microwave phonons are generated by spin precession, spin wave resonance and by the piezoelectric effect. In the case of magnetic generation, the particular phonon modes produced depend on the magnetic characteristics of the ferromagnetic transducer.

Experiments have been carried out on various compositions of Nb-Zr alloy wire and cylinders made of sintered Nb-Sn powders to determine their applicability to high-field superconducting magnets. In all cases of the Nb-Zr wire, the current-carrying capacity of short samples was found to fall off sharply at about 70 kgauss; the highest field generated so far from solenoids made from corresponding materials was 56 kgauss. A number of problems concerned with insulation and flexing of the wire have become evident. For the case of sintered Nb-Sn cylinders, current densities of at least 10^5 amp/cm^2 have been carried, which is comparable to values reported for NbSn-core wire.

A number of properties of materials in the superconducting state are being studied by means of phonon interactions. Initially, pulsed ultrasonic attenuation measurements at 30 Mcps have been carried out in niobium as a function of temperature.

The resonance condition for spiral spin configurations has been derived; it shows that it should be possible to excite magnetic resonance by a uniform RF magnetic field.

Benjamin Lax
Head, Division 8

H.C. Gatos
Associate Head

15 January 1962

VI. TRANSITION-METAL COMPOUNDS

Although the magnetic properties of the transition-metal compounds continue to occupy paramount interest, investigations of their transport properties have also begun. The motivation here is to study the properties of narrow-band electrons as the interatomic spacing decreases from a value in which they are localized to one in which they are collective. In one limit, ligand-field and electron-diffusion theory are applicable, in the other the molecular-orbital band theory is applicable. No satisfactory theory has been established for the intermediate region. Initial investigations of transport properties have been on various vanadium spinels. The magnetic properties of

vanadium spinels are also of interest, both because of the relatively strong B-site V-V exchange and because of the strong spin-orbit coupling associated with V^{3+} and V^{4+} ions. The B-site Cr-Cr interactions in chromium spinels are also relatively strong so that these, together with the vanadium spinels, provide examples of complex noncollinear spin configurations of the type studied theoretically and reported in previous Solid State Quarterly Progress Reports. Studies of transport properties will require the growth of chemically controlled single crystals, and two methods have been developed for growing single crystals of cobalt ferrite with nearly zero Fe^{2+} content.

Compounds with the nickel-arsenide structure also have interesting magnetic and electric properties. Again careful chemistry and crystallography is most important for the characterization of the materials, since the structure readily accommodates both cation defects and cation interstitials. For the study of 3d electrons, the system Cr_xS represents a localized-electron case, MnP a collective-electron case and FeS an intermediate case.

The bronzes represent a unique electron-transport problem. It is hoped that a range of composition can be made which will permit variation of the number of charge carriers without altering their mobility too greatly.

VII. MAGNETIC FILMS

Dispersion in the magnitude and direction of the local anisotropy in a magnetic film results in a fundamental limitation on the engineering performance in a computer memory. It has been shown that the dispersion of memory films is minimum at the zero-magnetostriction composition and hence that a major contribution to dispersion can be attributed to isotropic strain. Consequently the isotropic strain in memory films has been studied as a function of substrate temperature and rate of deposition. The principal result obtained was that the isotropic strain goes through zero near 300°C; above this temperature it is tension, below it compression. This suggests that there should be a minimum in dispersion as a function of substrate temperature, and this is being checked experimentally.

Dispersion is also being studied by considering films in which the dispersion is so great that the magnetic behavior is dominated by the dispersion rather than by the uniaxial anisotropy. There are several classes of these so-called anomalous films, but one common characteristic is the presence of isotropic rotational hysteresis in intermediate fields. A report on methods of preparation and the properties of these films will be completed next quarter. The various classes of films have been interpreted as due to the presence of high-anisotropy centers of varying density.

A system of magnetic domain-wall logic has been studied experimentally and the basic feasibility demonstrated.

VIII. SEMICONDUCTOR COMPONENTS

An additional ten state-of-the-art UHF switches of somewhat modified design from Texas Instruments Incorporated have been evaluated. These show improved DC characteristics and low-current frequency response. The high-current frequency response is essentially unchanged, but minority-carrier storage and base resistance have increased somewhat. It is becoming increasingly more difficult to obtain satisfactory measurements at the higher frequencies required. These units have f_T values at 3 volts and 20 ma which range from 3 to 5 kMcps.

The analysis of the behavior of "collecting" p-n junctions at high currents is continuing. In particular, a first-order solution has been obtained which describes the physical behavior of a linearly graded collecting p-n junction as a function of current density.

J. B. Goodenough
Leader, Group 53

D. O. Smith
Associate Leader

IX. OPTICS AND INFRARED

A general analysis of the solid state infrared image converter has yielded optimum design values for the frequency of the source voltage and the dimensions and physical constants of the photoconductive and electroluminescent layers.

Theoretical calculations indicate that parametric oscillation and amplification are possible at optical frequencies. A simple model is analyzed and experiments are now in progress to verify the predictions.

R. H. Kingston
Leader, Group 26

F. L. McNamara
Associate Leader

TABLE OF CONTENTS

PUBLISHED REPORTS OF AUTHORS FROM SOLID STATE RESEARCH

15 October 1961 through 15 January 1962

G-Report

No.				ASTIA and Hayden No.
81G-1	Broadening in the Master Equation	P.L. Kelley	25 October 1961	ASTIA 266360 H-352

Technical Reports

TR No.				
252	Elementary Lattice Theories and Their Application to Gas Adsorption Phenomena	J.M. Honig	11 December 1961	Unclassified
254	Ferro- and Antiferromagnetism in a Cubic Cluster of Spins	G.F. Dresselhaus	11 January 1962	Unclassified

Journal Articles*

JA No.			
1392A	The Oxidation of Intermetallic Compounds IV. The Sorption of Oxygen by InSb at 78°K	A.J. Rosenberg† A.A. Menna‡	Proceedings of the Fourth International Symposium on the Reactivity of Solids, Amsterdam (1960)
1478	Solid State Microwave Devices	R.H. Kingston	Nachrichtentechnische Fachberichte 22 (1961)
1664A	Calibration of Prism Spectrometers in the Ultraviolet, Visible and Near-Infrared Regions	S. Zwerdling J.P. Theriault	Spectrochim. Act. 17, 819 (1961)
1721	Relationship Between Crystal Symmetry and Magnetic Properties of Ionic Compounds Containing Mn^{3+}	J.B. Goodenough A. Wold R.J. Arnott N. Menyuk	Phys. Rev. 124, 373 (1961)
1730	Cryosar Memory Design	R.C. Johnston	Trans. IRE, PGEC EC-10, 712 (1961)
1744	Growth of Refractory Crystals Using the Induction Plasma Torch	T.B. Reed	J. Appl. Phys. 32, 2534 (1961)
1759	Some Effects of Anisotropy on Spiral Spin Configurations with Application to Rare-Earth Metals	T.A. Kaplan	Phys. Rev. 124, 329 (1961)

---

*Reprints available.

†Consultant.

‡Author not at Lincoln Laboratory.

Journal Articles (Continued)

JA No.			
1766	Impurity Striations in Unrotated Crystals of InSb	H.C. Gatos A.J. Strauss M.C. Lavine T.C. Harman	J. Appl. Phys. 32, 2057 (1961)
1777	Elements of Order-Disorder Theory – Applications to Gas Adsorption, Binary Solutions, Alloys, and Ferromagnetism	J.M. Honig	J. Chem. Educ. 38, 538 (1961)
1780	Cyclotron Resonance	B. Lax	Science 134, 1333 (1961)
1785	Magnetotunneling in Lead Telluride	R.H. Rediker A.R. Calawa	J. Appl. Phys. 32S, 2189 (1961)
1795	Oscillatory Magnetoabsorption in InSb Under High Resolution	S. Zwerdling W.H. Kleiner J.P. Theriault	J. Appl. Phys. 32S, 2118 (1961)
1799	Proposal for Magnetic Domain-Wall Storage and Logic	D.O. Smith	Trans. IRE, PGEC EC-10, 708 (1961)
1835	Mechanical Developer for Mass Spectrographic	E.B. Owens	Rev. Sci. Instr. 32, 1420 (1961)
1854	Low Electron Effective Masses and Energy Gap in $Cd_xHg_{1-x}Te$	T.C. Harman A.J. Strauss D.H. Dickey M.S. Dresselhaus G.B. Wright J.G. Mavroides	Phys. Rev. Letters 7, 403 (1961)
General	Exciton and Magneto-Optical Effect in Unstrained Germanium	D.F. Edwards V.J. Lazazzera* C.W. Peters*	Proc. Conf. Semicond. Phys., Prague, J4, 335 (1960)
General	The Interaction of NO_2-N_2O_4 and Certain Metallic Oxides: Terbium Sesquioxide, Lanthanum Oxide, Vanadium Sesquioxide and Perovskite Phase $PrCrO_3$	F. Vratny†	J. Inorg. Nucl. Chem. 21, 77 (1961)
General	The Interaction of NO_2-N_2O_4 and Barium, Sodium and Silver Nitrites	F. Vratny† F. Gugliotta*	J. Inorg. Nucl. Chem. 20, 252 (1961)
MS-22	Magneto-Spectroscopy in Semiconductors	B. Lax	Proc. Conf. Semicond. Phys., Prague, J1, 321 (1960)
MS-24	Damaged Layers in the {111} Surfaces of the III-V Semiconductor Compounds	H.C. Gatos M.C. Lavine E.P. Warekois	Proc. Conf. Semicond. Phys., Prague, M9, 519 (1960)

*Author not at Lincoln Laboratory.

†Consultant.

Journal Articles (Continued)

JA No.			
MS-26	Impact Ionization of Impurities in Compensated Germanium	A.L. McWhorter R.H. Rediker	Proc. Conf. Semicond. Phys., Prague, D10, 134 (1960)
MS-94	Spin-Lattice Interaction for Electrons in Semiconductors	L.M. Roth	Proc. Conf. Semicond. Phys., Prague, N4, 592 (1960)
MS-268	Band Structure of HgSe and HgSe-HgTe Alloys	T.C. Harman A.J. Strauss	J. Appl. Phys. 32S, 2265 (1961)
MS-269	Magnetoreflection Experiments in Intermetallics	G.B. Wright B. Lax	J. Appl. Phys. 32S, 2113 (1961)
MS-270	Interband Faraday Rotation in III-V Compounds	B. Lax Y. Nishina	J. Appl. Phys. 32S, 2128 (1961)
MS-347	Statistical Mechanics of Dilute Solid Solutions	R.F. Brebrick	J. Appl. Phys. 33S, 422 (1962)
MS-394	Superconducting Magnets	S.H. Autler	NEREM Record 3 (November 1961)

* * * * *

UNPUBLISHED REPORTS

Journal Articles

JA No.			
1783	Preparation of Stoichiometric Chromites	E. Whipple A. Wold	Accepted by J. Inorg. Nucl. Chem.
1796	Noncoherent Switching in Permalloy Films	D.O. Smith K.J. Harte	Accepted by J. Appl. Phys.
1812	Electrochemical and Adsorption Measurements on Single Crystals: The Germanium-Iodide Solution System	W.W. Harvey W.J. LaFleur H.C. Gatos	Accepted by J. Electrochem. Soc.
1820	Interband Transitions for Metals in a Magnetic Field	M.S. Dresselhaus G.F. Dresselhaus	Accepted by Phys. Rev.
1828	Non-Parabolic Conduction Band in HgSe and $HgSe_{0.5}Te_{0.5}$	G.B. Wright A.J. Strauss T.C. Harman	Accepted by Phys. Rev.
1835	Mechanical Developer for Mass Spectrographic Plates	E.B. Owens	Accepted by Rev. Sci. Instr.
1840	Interband Transitions in Superconductors	G.F. Dresselhaus M.S. Dresselhaus	Accepted by Phys. Rev.
1852	Vapor Growth of Tin Oxide Crystals	T.B. Reed J.T. Roddy A.N. Mariano	Accepted as Letter to the Editor, J. Appl. Phys.

Journal Articles (Continued)

JA No.			
1864	{100} Facets in Pulled Crystals of InSb	A.J. Strauss	Accepted by Solid-State Electronics
1869	On the Theory of Tunneling and Its Dependence on a Longitudinal Magnetic Field	P.N. Argyres	Accepted by Phys. Rev.
1878	Simple Vacuum – He II Tight Optical Windows	C.J. Rauch W.C. Kernan	Accepted as NOTE, Rev. Sci. Instr.
1888	Infrared Oscillations from CaF_2: U^{+3} and BaF_2: U^{+3} Masers	H.A. Bostick J.R. O'Connor	Accepted by Proc. IRE

Meeting Speeches*

MS No.			
251	Heat Transfer Intensity Distribution in Induction Plasma Flames	T.B. Reed	ASME Plasma Jet Symposium, New York, 26 November – 1 December 1961
294	The Role of Crystalline Structure in Surface Reactivity	H.C. Gatos	American Institute of Chemical Engineering, New York, 5 December 1961
312	Distribution of Sulfur Impurity in InSb Single Crystals	M.D. Banus H.C. Gatos	Semiconductor Symposium, Detroit, 2-3 October 1961
350	Cobalt Ferrite Crystal Growth from the Ternary Flux System Na_2O-CoO-Fe_2O_3	W. Kunnmann A. Wold E. Banks	Conference on Magnetism and Magnetic Materials, Phoenix, 13-16 November 1961
351	Vanadium Iron Oxides	A. Wold D. Rogers R.J. Arnott N. Menyuk	
352	A Microwave Magnetic Microscope	R.F. Soohoo	
353	Antiferromagnetic Resonance in $MnTiO_3$	J.J. Stickler G.S. Heller	
356	Isotropic Stress Measurements in Evaporated Permalloy Films	G.P. Weiss D.O. Smith	
361	Magnetic Properties of Mixed Vanadium-Chromium Sulfides	K. Dwight R.W. Germann A. Wold N. Menyuk	

* Titles of Meeting Speeches are listed for information only. No copies are available for distribution.

Meeting Speeches (Continued)

MS No.			
362	Magnetic Transitions in Cubic Spinels	N. Menyuk A. Wold D.B. Rogers K. Dwight	Conference on Magnetism and Magnetic Materials, Phoenix, 13-16 November 1961
363	Cation- -Cation Three-Electron Bonds	J.B. Goodenough	
382	Proposal for and Demon ·ration of Magnetic Domain-Wall Storage and Logic	J.M. Ballantyne	
441	High Magnetic Field Research	B. Lax	
358	Flux Concentration by Stationary Conductors	B. Howland* S. Foner	International Conference on High Magnetic Fields, M.I.T., 1-4 November 1961
359	Magneto-Optical Phenomena in Solids	B. Lax	
367	Superconducting Magnets	S.H. Autler	
384	Chemical Bonding and Surface Behavior	H.C. Gatos	Colloquium on Surface Phenomena, M.I.T., 21 November 1961
385	The Role of Crystallographic Polarity in the Behavior of Single Crystals	H.C. Gatos	Physics Colloquium, Brown University, 23 October 1961
393	Crystal Growth at Lincoln Laboratory	T.B. Reed	Symposium on Single-Crystal Growth, M.I.T., 30 November 1961
399	Problems in Processing and Upgrading Properties of Electronic Materials	E.P. Warekois	Ceramics Colloquium, M.I.T., 20 October 1961
400	Electronic Materials	H.C. Gatos	Experimental Methods in Metallurgy, M.I.T., 30 October 1961
405	Principles and Applications of Superconducting Magnets	S.H. Autler	Boston Section of AIEE, M.I.T., 28 November 1961
406	Electrodeless Thermal Plasma Techniques	T.B. Reed	American Society for Metals, Oak Ridge, 8 November 1961
414	Superconductivity and the Generation of Intense Magnetic Fields	S.H. Autler	Physics Colloquium, Columbia University, 15 December 1961
421	The Characteristics of Semiconductor Surfaces	W.W. Harvey	Colloquium on Surface Phenomena, M.I.T., 5 December 1961

* Division 5.

Meeting Speeches (Continued)

MS No.			
430	Millimeter Cyclotron Resonance in Diamond	C.J. Rauch	Seminar at RCA Laboratories, Princeton, 15 November 1961
442	Low Temperature Semiconductors and Semimetals	B. Lax	Colloquium at Texas Instruments, Dallas, 14 December 1961
443	Electron Ordering Transitions in Transition-Element Compounds	J.B. Goodenough	Colloquium, Syracuse University, 10 December 1961
450	Comments on the 3d Electron Problem	J.B. Goodenough	Colloquium, University of Minnesota, 11 January 1962
452	Solution of Schrödinger Equation for a Periodic Lattice	L. Eyges	Winter Institute in Quantum Chemistry and Solid State Physics, University of Florida, 7-13 January 1962

For convenience in ordering copies of Lincoln Laboratory reports cited in this document, each reference is followed by its ASTIA number. In addition, Unclassified (released) reports have also been assigned Hayden serials (designated H-), indicating that they are obtainable, at cost, as microfilm or photoprint copies from the Micro-Reproduction Service, Hayden Memorial Library, M.I.T., Cambridge 39, Massachusetts.

ORGANIZATION LIST

DIVISION OFFICE

Benjamin Lax, *Division Head*
Harry C. Gatos, *Associate Head*
M. J. Hudson, *Assistant*
D. T. Stevenson
S. Zwerdling

GROUP 81

J. M. Honig, *Leader*
T. C. Harman, *Assistant Leader*

Argyres, P. N.
Brebrick, R. F.
Brown, M. C.
Cella, A. A.
Dibley, D. B.
Dresselhaus, G. F.
Durgin, M. G.
Eyges, L. J.
Hilsenrath, S.
Honig, N. J.*
Kelley, P. L.†
Kern, S.*
Kleiner, W. H.
Mason, V. J.
Pratt, G. W., Jr.*
Quelle, F. W.*
Rawson, N. B.
Roth, L. M.
Sherman, A. M.*
Sillers, S. J.

GROUP 82

G. S. Heller, *Leader*
H. J. Zeiger, *Associate Leader*
P. E. Tannenwald, *Assistant Leader*

Autler, S. H.
Catuna, G. W.
Feldman, B.
From, W. H.
Kernan, W.
Mills, E. D.
Momo, L. R.*
Rauch, C. J.
Rosenblum, E. S.
Seavey, M. H., Jr.
Stickler, J. J.
Thaxter, J. B.
Walters, E.
Weber, R.*

GROUP 83

E. P. Warekois, *Leader*
A. J. Strauss, *Assistant Leader*

Banus, M. D.
Button, M. J.
Carter, F. B.
Cornwell, J. C.
Farrell, L. B.
Finn, M. C.
Fischler, S.
Gardels, M. C.
Giardino, N. A.
Hanneman, R. E.†
Harvey, W. W.
Kafalas, J. A.
LaFleur, W. J.
Lavine, M. C.
Mariano, A. N.
Nye, S. D.
Owens, E. B.
Peacor, D. R.‡
Plonko, M. C.
Reed, T. B.
Roddy, J. T.
Turnbull, T. P.
Vose, D. W.

GROUP 84

J. G. Mavroides, *Leader*

Brown, R. N.
Button, K. J.
Curran, E. A.
Dickey, D. H.
Dresselhaus, M. S.
Edwards, D. F.
Kolesar, D. F.
Krag, W. E.
Scouler, W. J.
Theriault, J. P.
Wright, G. B.

GROUP 85

R. H. Rediker, *Leader*
R. H. Kingston, *Acting Assistant Leader*

Calawa, A. R.
Dennis, J. H.
Dominick, F. J.
Grant, C. R.
Halpern, J.†
Hamann, D. R.‡
Hurwitz, C. E.†
Keyes, R. J.
Lowen, J.
May, W. G.‡
McWhorter, A. L.*
Melngailis, I.
Quist, T. M.
Ward, J. H. R., III

---

*Part Time
†Staff Associate
‡Leave of Absence

A. THE DOUBLY AND TRIPLY IONIZED STATES OF COPPER IN GERMANIUM

The practical application of the photoconductive properties of copper impurities in germanium for the conversion of infrared images into visible pictures was described in a previous report.[1] Although compensated copper-doped germanium crystals were incorporated in this device, very little was known about the details of the photoconductive and infrared absorptive process of the doubly and triply ionized levels of copper. An experimental measurement program was initiated in the last quarter in order to obtain information concerning the following parameters of the copper impurities in germanium:

(1) The wavelength dependence of the photoconductivity,
(2) The wavelength dependence of the absorption cross section,
(3) The relaxation times associated with the recombination of excited carriers.

There are three basic reasons for initiating this measurement program. First, these parameters are necessary for the proper design of infrared devices that might incorporate these impurities. Second, very little is known about the location in $\vec{k}$ space of the bound states of non-hydrogen-like impurities in germanium. Since copper in germanium is such an impurity, it seemed that the proposed measurements would shed some light on this much-neglected area. Third, it was hoped that, as a result of these measurements, one could ascertain whether or not a CW infrared laser could be made to function via deep impurity levels in germanium. Unfortunately the measurements performed to date have introduced new problems as well as shedding light on the existing ones.

An energy band diagram for the compensated copper impurities in germanium is shown in Fig. I-1. From Hall measurements as a function of temperature, the energy position of the various ionization states of copper are[2] 0.04, 0.32 and 0.26 electron volt (ev) as indicated in the figure.

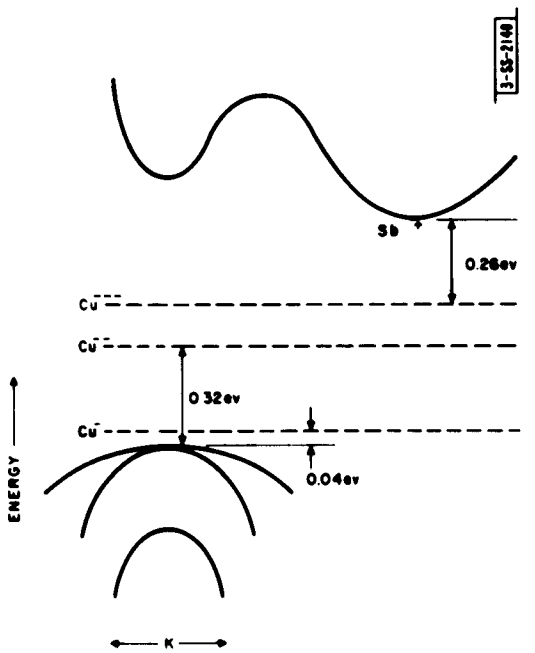

Fig. I-1. Energy band diagram of Ge showing the copper levels.

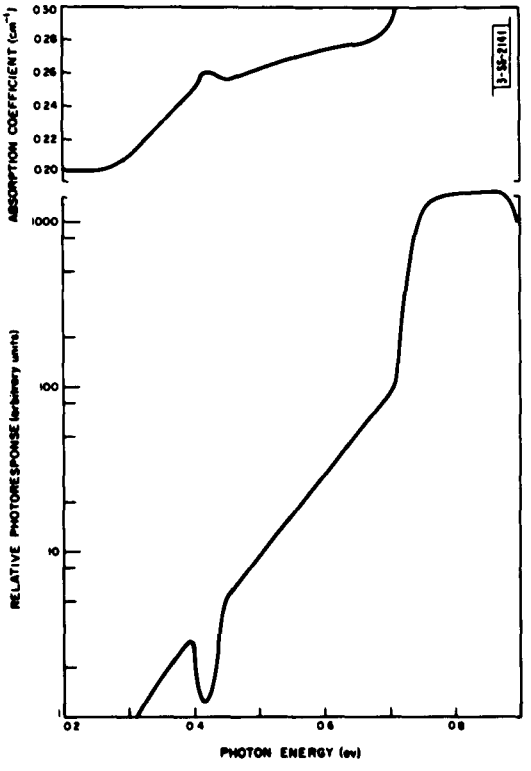

Fig. I-2. Photoresponse and absorption as a function of photon energy for the Cu^{--} level. The sample (1050-1) is 2 mm thick and has a copper concentration of 1.5×10^{15} cm^{-3}.

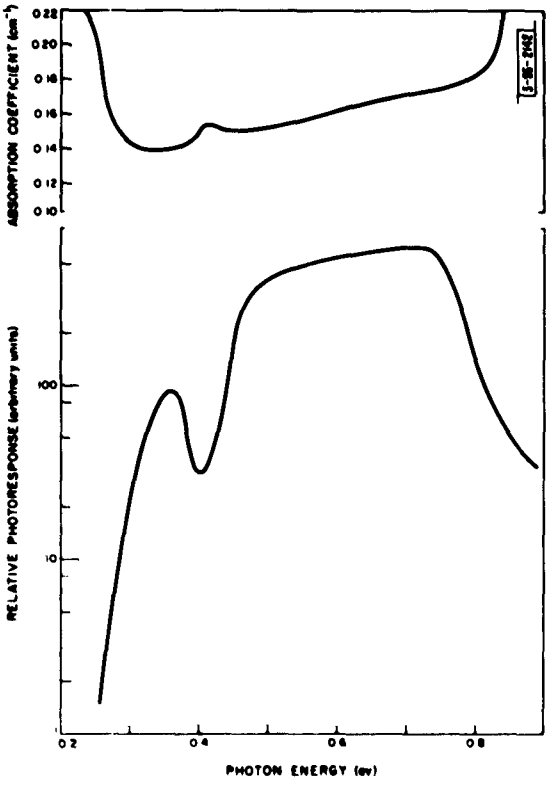

Fig. I-3. Photoresponse and absorption as a function of photon energy for the Cu^{---} level. The sample (SM-10) is 5 mm thick and has a copper concentration of 1.2×10^{15} cm^{-3}.

As previously stated, the $\vec{k}$ values to be associated with the impurity levels are uncertain. For simplicity the copper impurity levels have been drawn as being independent of $\vec{k}$.

Figures I-2 and I-3 show the photoconductivity and absorption coefficient as a function of photon energy for doubly and triply ionized copper samples, respectively, both at 78°K. The samples were prepared by diffusing copper into antimony-doped germanium crystals. The density of copper in the crystals was controlled by the diffusion temperature. In the Cu^{--} sample the density of antimony atoms is greater than the density of copper atoms, but less than twice the copper density. In the Cu^{---} sample the antimony density is greater than twice the copper density, but less than three times the copper density. The Cu^{--} sample has a threshold in photoconductivity at approximately 0.32 ev which agrees with values obtained from thermal measurements. The absorption of this sample also has an edge at 0.32 ev in agreement with the absorption data of Greenway.[3] However, in our samples a broad weak absorption line occurs at 0.41 ev accompanied by a large decrease in photoconductivity at this energy. The magnitude of the absorption line increases with the amount of near-infrared radiation impinging on the sample. At present it appears that this line is due to levels introduced by crystal imperfections, which also produce a photoconductive quenching action in the crystal.

The measurements on Cu^{---} crystals also yield a threshold of photoconduction as a function of photon energy which verifies the existence of the Cu^{---} level at 0.26 ev below the conduction band. The same broad absorption and quench line appear at 0.41 ev as was observed in the Cu^{--} sample. The absorption curve for this sample, however, shows a decrease in absorption at 0.26 ev, and does not agree with Greenway's data. At present it is impossible to reconcile the absorption curve with the photoconductive data for our Cu^{---} sample. It does not make sense to have a maximum in photoconduction when the absorption is a minimum. It should be pointed out that the absorption data of Greenway and our photoconductivity data for the Cu^{---} level are compatible.

The lifetime of the photoexcited carriers in both the Cu^{---} and Cu^{--} crystals was found to range between 0.5 and 2×10^{-3} second when excited by visible radiation. Excitation by penetrating infrared radiation gave the same lifetime as the visible excitation in the Cu^{---} crystals but a lifetime too short to be measured by pulse techniques in the Cu^{--} crystals. In this latter case the lifetime deduced from steady-state techniques yields values in the range of 10^{-7} second.

The photoconductivity, absorption and thermal activation energy measurements are in general agreement for the Cu^{--} level in germanium. The qualitative shapes of the curves suggest that the Cu^{--} energy level does not have a discrete $\vec{k}$ value. In order to obtain a more quantitative picture of the level structure, similar measurements are being performed on samples with different degrees of compensation and copper content.

R. J. Keyes

B. FABRICATION OF PbSe TUNNEL DIODES

PbSe tunnel diodes have been fabricated by abruptly alloying indium spheres onto Ag-doped p-type PbSe having an impurity concentration of from 1×10^{18} cm^{-3} to 8×10^{18} cm^{-3} and mobilities of 5×10^{3} cm^{2}/volt-sec to 2×10^{4} cm^{2}/volt-sec both at 77°K. The alloying is done on a low-heat-capacity carbon-strip heater, the heating and cooling of which is automatically controlled. The junction alloy cycle time is approximately 2 seconds, reaching a peak temperature of about 250°C. The base contact is made by alloying the PbSe to an Au-clad Ta tab, using an In-Au wafer containing 1 per cent Au. Because of the higher temperature required to bond the

PbSe to the tab and because of the high vapor pressure of Se, it was necessary to make the ohmic contact first and to etch and clean the PbSe between each step of the process. The PbSe wafers previously lapped with 10-micron alumina are electrolytically etched for 30 seconds prior to bonding to the base tab, for 20 seconds prior to forming the alloy junction and for 10 seconds after the device is mounted on a header. The etching is done in a solution of 100 ml phosphoric acid and 10 grams chromic acid,[4] using a current density of approximately 3 amp cm^{-2}. The solution temperature should be kept between 75° and 85°C. After etching from 10 to 30 seconds, an orange film is formed on the surface which can be wiped off with a cotton-tipped applicator and a 10 per cent KOH-H_2O solution. The film can also be removed ultrasonically in the 10 per cent KOH-H_2O solution. The orange color of the film formed is a clear indication of the proper etching parameters. Excessive chromic acid, too high a current density or too high a solution temperature results in a red film and a poor PbSe surface. Deficient chromic acid, too low a current density or solution temperature results in a yellow film and again a poor PbSe surface. The final step is to rinse the sample thoroughly in deionized water.

It has not been possible to obtain the negative conductance characteristic of tunnel diodes at forward biases, and the resultant unilateral nonlinear characteristic is easily confused with contact or surface effects. To be certain that tunneling did contribute the major portion of the diode current, a conductance plotter[5] is used. If tunneling is predominant, conductance-voltage traces at 4.2°K clearly show a polaron minimum at V = 0 and the optical phonon bump at V ≈ 16 mv (Ref. 6).

A. R. Calawa

C. EPITAXIAL GROWTH

Our present objective is to grow a uniform p-type layer of boron-doped germanium onto an n-type substrate of germanium. The high temperatures, 840° to 850°C, needed for growth of a polished surface layer thermally convert the n-type germanium to p-type material. This can be reconverted to its original type and resistivity by evaporating indium onto the bottom of the wafer and annealing for one hour at 650°C, followed by a slow decrease to room temperature.

Table I-1 illustrates the results of the above-described method of epitaxial growth. As can

TABLE I-1
RESULTS OF EPITAXIAL GROWTH

Sample No.	Growth Time (minutes)	Junction Depth (mils)	n-type Base Material		p-type Epitaxial Layer (ohm-cm)	Doped $GeCl_4$ Source*
			Original (ohm-cm)	Final (ohm-cm)		
60	12	0.8	0.4	0.5	3.0 – 4.8	A
61	130	3.0	0.4	0.4	1.7 (very uniform)	A
62	12	0.7	0.4	0.4	3.0 – 9.0	A
63	12	0.8	0.4	0.4	3.0 – 9.0	A
69	20	0.8	1.0	2.0	0.8 – 1.2	B
70	20	0.7	1.0	1.0	3.0 – 5.2	B
72	30	0.8	1.0	1.0	4.0 – 7.0	B

* Source B was doped with five times the amount of BCl_3 as source A.

be seen from the table, the deposition rate is uniform and fairly reproducible. The uniformity and reproducibility of the resistivity of the epitaxial layer, however, leaves much to be desired.

J. Lowen

D. NEGATIVE RESISTANCE InSb DIODES WITH LARGE MAGNETIC-FIELD EFFECTS

A large negative resistance region has been observed in the forward characteristics of n^+p InSb diodes in which the thickness of the p-base is large (>1 mm) compared with the minority carrier diffusion length for low injection levels. Figure I-4 shows the forward current-voltage characteristic at 77°K of such a diode. For this diode the resistivity of the p-base at 77°K is 40 ohm-cm and varies with temperature with an activation energy of 0.055 ev. The negative resistance region has also been observed for diodes in which the resistivity of the p-base is 4 ohm-cm and nearly independent of temperature about the operating range of 77°K. For identical geometry the negative resistance is larger for higher base resistivity (up to 160 ohm-cm at 77°K has been investigated) and for all diodes is enhanced by reducing the operating temperature. Less than 10^{-7} second has been required to switch the state of experimental units either from the high-impedance state to the low-impedance state, or vice versa.

In order to investigate the phenomena involved in producing the negative resistance, a bar-shaped sample was made with rectifying and ohmic contacts on opposite ends and three potential probe contacts along the sides as shown in Fig. I-5. Also shown in this figure are the voltages V_1, V_2 and V_3 across the different portions of the bar as a function of diode current. Note that there is a negative resistance region in each part of the bar and that the "breakdown" point occurs at progressively higher diode currents in parts farther away from the rectifying junction. The small-signal conductance between probes on opposite sides of the bar was also measured as a function of diode current. As the diode current was increased, the conductance increased first in regions close to the diode, whereas no change was observed between probes farther along the bar. At higher currents the conductance change propagated down the length of the bar toward the ohmic contact. These experiments suggest that the negative resistance is associated with an abrupt change of the conductivity modulation in the base produced by minority carrier injection from the rectifying junction. The "breakdown" point does not occur at a critical value of current density or electric field in the base, but rather seems to depend on the density of injected carriers.

As a consequence of trapping, electron lifetimes in p-type InSb at 77°K are as short as 5×10^{-10} sec at low injection levels.[7,8] Since longer lifetimes than this are necessary to produce the strong conductivity modulation following breakdown in these "long-base" diodes, the negative resistance appears to result from an increase of injected carrier lifetime[9] as the traps are filled by sufficient injection. As expected from this model, injecting minority carriers with white light increased the prebreakdown conductance and greatly reduced the breakdown voltage. Tyler[10] has also seen a breakdown effect in p^+n Ge diodes at 77°K in which the n-region had been Fe-doped. His explanation that the conductivity after breakdown is due to mobile majority carriers which neutralize the trapped minority carriers is part of the above explanation. But in our case the lifetime change seems to play a crucial role. For Tyler's samples, when the I-V characteristic is swept at 60 cps, after the first breakdown the negative resistance region disappears and breakdown occurs at the sustaining voltage. This might be expected because of the longer carrier lifetimes in Ge.

The I-V characteristic of the negative resistance InSb diodes is extremely sensitive to magnetic fields perpendicular to the direction of current flow in the base region. As can be seen

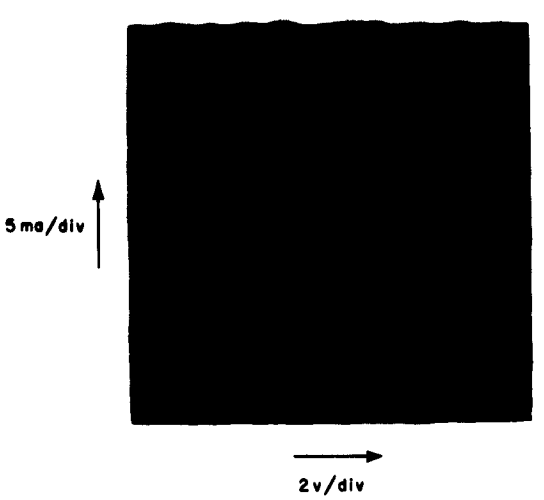

Fig. I-4. Forward current-voltage characteristic of an InSb n^+p diode with a bar-shaped base region $1.0 \times 0.5 \times 0.5$ mm of 40 ohm-cm resistivity. The junction current density at the "breakdown" point is 0.8 amp cm^{-2}.

Fig. I-5. The abscissa is the voltage across different portions of the bar-shaped 25 ohm-cm base region of an n^+pp^+ diode. The ordinate is the diode current. The placement of the voltage probes on the base region is illustrated in the figure.

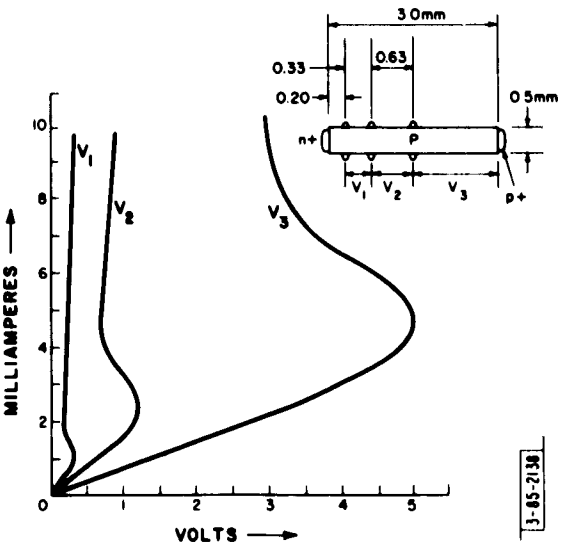

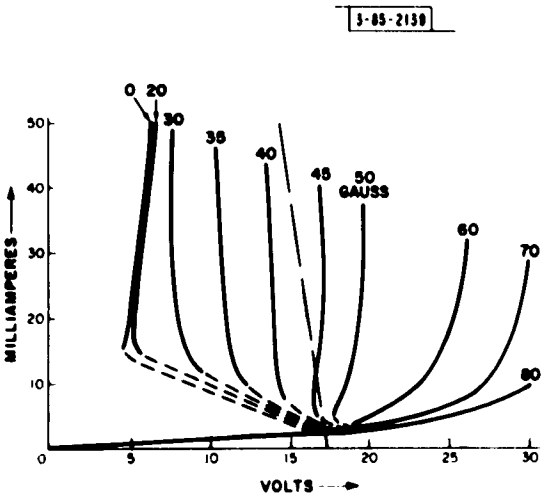

Fig. I-6. Effect of different magnetic fields perpendicular to the current flow on the forward current-voltage characteristic of an InSb n^+p diode with a bar-shaped base region $1.5 \times 0.5 \times 0.5$ mm of 40 ohm-cm resistivity. For the load line shown dashed, the diode current is changed by almost 50 ma by a magnetic field change of less than 5 gauss.

from Fig. I-6, the magnetic field greatly increases the resistance after breakdown. Less than 10 gauss has been used to switch the state of experimental devices such as that of Fig. I-6. As can be seen from the figure, if the device is operated with a quiescent magnetic field of 40 gauss and the load line as shown, the application of 5 additional gauss will change the current by almost 50 ma. Although the devices have by no means been optimized as yet for maximum magnetic-field effect, the magnetic effect is clearly larger than that we have reported[11] for InSb n^+p diodes of lower base resistivity.

The effect of the magnetic field is to decrease the minority carrier diffusion length and hence the conductivity modulation of the base region. Karakushan, et al., have described[12] the decrease in the diffusion length due to a reduction of the carrier mobility by the magnetic field. The diffusion length can also be made smaller by reducing the carrier lifetime either by deflecting the carriers from the region where the lifetime has been increased because the traps have been saturated, to lower lifetime regions, or by deflecting the carriers to the surface (the Suhl effect[13]). Our results (Sec. I-E) indicate that the reduction in effective lifetime is more important than the reduction in mobility.

I. Melngailis

E. SUHL EFFECT IN p-TYPE InSb

If opposite faces of a bar-shaped base region are subjected to a different surface treatment, and a magnetic field is applied transverse to the diode current and parallel to these faces, then the magnetic sensitivity is different for magnetic fields of opposite polarity. This suggests that minority carriers are deflected toward the surfaces in a manner first observed by Suhl in germanium.[13] With two-carrier conduction, the Hall voltage is minimized because both holes and electrons are deflected toward the same surface, preventing a charge buildup. For injected high mobility electrons in p-type InSb, the Hall angle already has a value of 16° at 50 gauss; hence a strong carrier concentration at the surface can be expected at low fields.

To measure conductance near the surface, two small closely spaced test probes were alloyed on a face of a bar as shown in Fig. I-7 (inset). A constant forward current of 11 ma was passed through the diode, and the conductance between the probes was measured by means of a small 1000-cps AC signal, while varying the transverse magnetic field. The resulting plot shows first an increase of conductance with positive B, as carriers are concentrated at the surface, followed

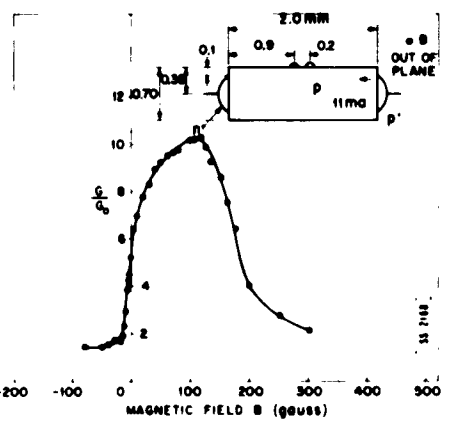

Fig. I-7. Conductance between surface probes as a function of magnetic field. G_o is the conductance between the probes with no minority carrier injection in the base. The inset gives the experimental sample for measuring conductance variation on the surface, showing direction of current and magnetic field.

by a decrease after a maximum has been reached. Suhl has shown that such a decrease is expected because carriers recombine on the surface before reaching the test point, if the field is sufficiently high. With negative magnetic fields, the conductance decreases as carriers are deflected away from the surface.

I. Melngailis

F. MAGNETIC EFFECTS ON InSb n-p-n TRANSISTORS

Alloyed n-p-n InSb transistors have been made with a base thickness of 0.2 to 1.0 mm. Preliminary tests show a large decrease of α in magnetic fields of the order of 50 gauss transverse to minority carrier flow in the base, as could be expected from the magnetic effects on minority carriers in n^+p diodes.

I. Melngailis

G. PHOTOCONDUCTIVITY OF Ge AT LOW TEMPERATURES

During the course of investigating the effect of light on the impurity conduction of compensated Ge at liquid helium temperatures, an apparently rather complex recombination mechanism was encountered. This recombination process is now being studied by measuring the time constant of the photoconductive response to a small chopped light signal as a function of the DC light bias, the temperature and the impurity concentrations.

J. H. R. Ward
A. L. McWhorter

REFERENCES

1. Quarterly Progress Report on Solid State Research [U], Lincoln Laboratory, M.I.T. (15 October 1961), p. 7, ASTIA 266878, H-360.
2. H.H. Woodbury and W.W. Tyler, Phys. Rev. 105, 84 (1957).
3. D.L. Greenway, Proc. Phys. Soc. (London) 76, 900 (1960).
4. P.H. Schmidt, J. Electrochem. Soc. 108, 104 (1961).
5. This instrument, built by T.M. Quist of this Laboratory, is a modification of an instrument described by J.J. Tieman, Rev. Sci. Instr. 32, 1093 (1961).
6. R.N. Hall and J.H. Racette, J. Appl. Phys. 32, 2078 (1961).
7. R.N. Zitter, A.J. Strauss and A.E. Attard, Phys. Rev. 115, 266 (1959).
8. R.A. Laff and H.Y. Fan, Phys. Rev. 121, 53 (1961).
9. V.I. Stafeev, Sov. Phys. Solid State 1, 763 (1959).
10. W.W. Tyler, Phys. Rev. 96, 226 (1954).
11. I. Melngailis, A.R. Calawa and R.H. Rediker, Bull. Am. Phys. Soc. Series II, 7, 88 (1962).
12. E.I. Karakushan and V.I. Stafeev, Sov. Phys. Solid State 3, 493 (1961).
13. H. Suhl and W. Shockley, Phys. Rev. 75, 1617 (1949).

II. CHEMISTRY

A. SURFACE STUDIES

1. Parallel Solution Conduction

The study of co-conduction by a solution in contact with a germanium wafer has been completed. Recent results provide additional confirmation of a general theory of the distribution of longitudinal current between an electrode and an electrolyte.[1] Thus the electrode potential measured between a reference electrode in the solution and a probe contact to the back surface of the wafer was found to vary as the difference in potential between the probe and the electrical contact to one end of the wafer. The form of the potential profile for the case of appreciable co-conduction is also in agreement with the predictions of theory.

Figure II-1 shows potential profiles for a p-type germanium wafer in contact with 0.1N H_2SO_4 and with 1.0M H_2O_2/0.1N H_2SO_4. The length of the germanium-electrolyte interface was 17 mm. For a longitudinal current of 2 ma, co-conduction by 0.1N H_2SO_4 was inappreciable, even though the potential difference between the extremes of the contact with the solution was approximately 0.9 volt. The reason is that, owing to the relatively broad plateau in the $j(\eta)$ characteristic for 0.1N H_2SO_4 (smooth germanium surface, Fig. II-2), a combined anodic and cathodic overpotential of this magnitude can be accommodated without appreciable electrolysis. Co-conduction by the same solution is greater for a longitudinal current of 4 ma; by reference to the appropriate $j(\eta)$ characteristic, the electrolytic current densities at the extremes of the contact with the solution are estimated to be in the range 2 to 3 ma cm^{-2}. Again by reference

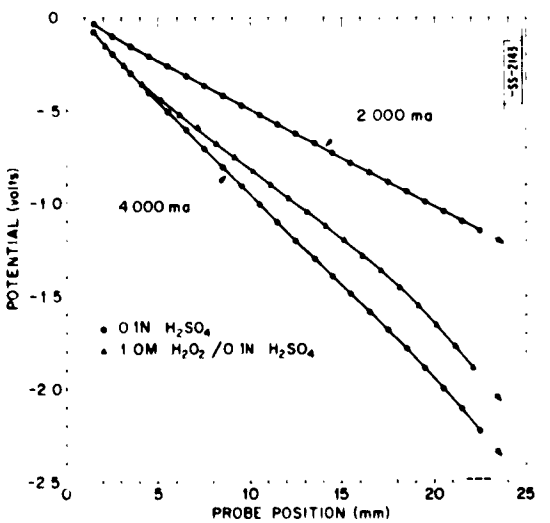

Fig. II-1. Variation of potential with distance along the back surface of a rectangular germanium wafer whose front surface contacts the solutions indicated, 22.5°C. Ge: p-type, {111}, 30 ohm-cm. The potentials indicated by --- refer to the potential difference between the ends of the wafer with distilled H_2O in contact with the front surface.

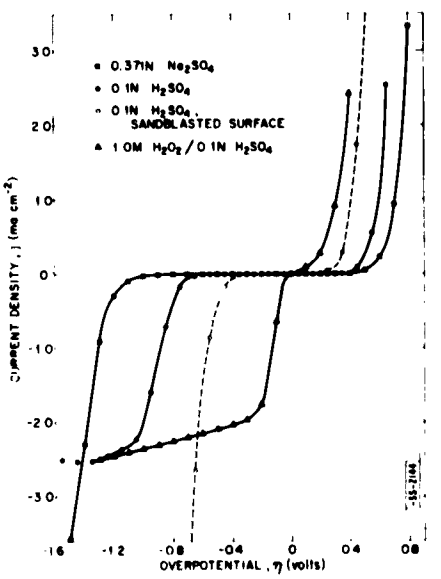

Fig. II-2. Electrolytic current density-overpotential characteristics for p-Ge electrodes in several solutions of interest, 300.0°K. Same electrode material as for Fig. II-1. Positive values of j and η correspond to anodic polarization.

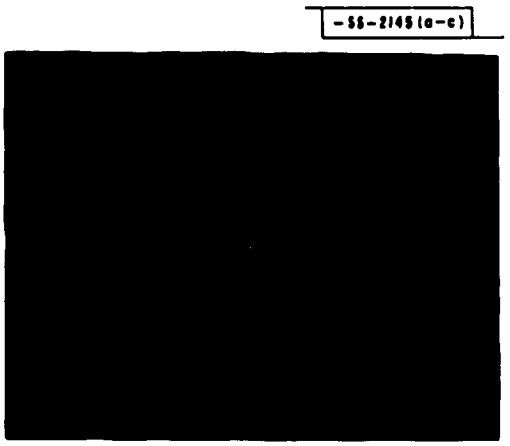

Fig. II-3(a). Region of a {111} germanium surface showing conical pits produced by etching in CP-4.

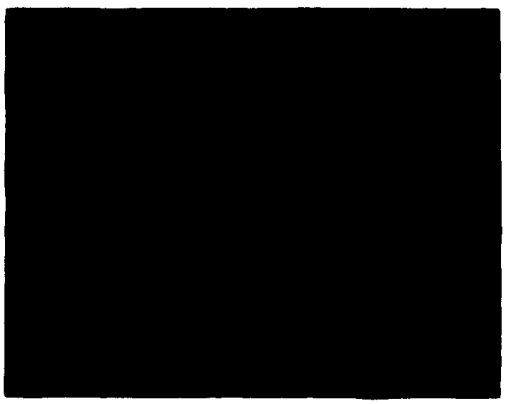

Fig. II-3(b). Same region following high-temperature etching in argon, 24 hours at 700°C.

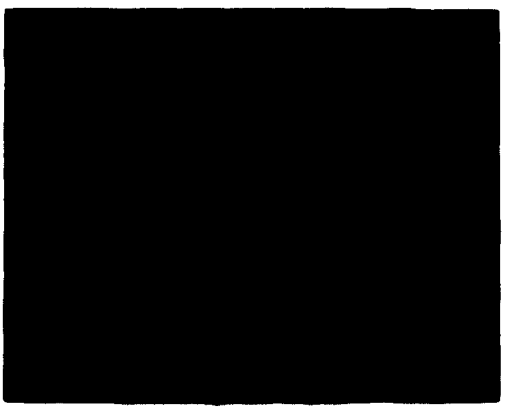

Fig. II-3(c). Same region after re-etching in CP-4. 125X.

to Fig. II-2, co-conduction in 0.1N H_2SO_4 which has been made 1.0 M in H_2O_2 is expected to be pronounced, as confirmed by the data of Fig. II-1.

It was indicated in the last quarterly progress report that, in principle, the distribution of potential and longitudinal current can be calculated from the measured $j(\eta)$ characteristic. The direct determination of the potential distribution (profile), when combined with the $j(\eta)$ characteristic, establishes the electrolytic current distribution without resort to theory.

W. W. Harvey

2. Limiting Electron Currents in p-Ge Electrodes

The electrolytic current density-overpotential characteristics shown in Fig. II-2 were obtained potentiostatically, allowing 30 seconds between settings. The limiting cathodic current shown for the 0.1N H_2SO_4 solution (smooth germanium surface) extended to an overpotential of -2.15 volts, the limit of the measurements. The rate of the cathodic reaction was found to be limited by the supply of electrons as evidenced by the following observations: Illumination of the electrode surface by means of a microscope lamp approximately doubled the limiting current; a 10°C rise in temperature increased the limiting current by a factor of 1.4; a limiting current was not attained when the electrode surface was sandblasted (see figure), but was restored by anodic dissolution of the work-damaged layer (20 microns of germanium removed). The foregoing marks the first instance of a stable limiting electron current in a p-type germanium cathode.

In oxygen-saturated 0.1N H_2SO_4, the same limiting electron current was observed to follow a limiting oxygen diffusion current of magnitude 0.17 ma cm^{-2}. In 0.1N H_2SO_4 containing 1.0 M H_2O_2, the limiting electron current was again observed, although in this case the cathodic reaction is reduction of H_2O_2 rather than hydrogen evolution. In the nearly-neutral Na_2SO_4 solution, where the species reduced is the water molecule, no limiting electron current was observed. Thus it appears that the cathodic reduction of H^+ and of H_2O_2 proceeds via the conduction band of the crystal, whereas cathodic reduction of H_2O involves the liberation of holes. Additional experiments are planned.

W. W. Harvey

3. High-Temperature Etching of Germanium

A correlation between pits formed during thermal treatment of germanium {111} surfaces and edge-type dislocations was established by using a replicating tape technique. Replicas were prepared (a) of the original CP-4 etched surface, (b) of the same surface after 24 hours at 700°C in an argon stream and (c) of the same surface after re-etching in CP-4. The replicas were superimposed, and photomicrographs were taken by focusing on each replica in turn, with the results shown in Figs. II-3(a-c). This technique lessened the difficulty of selecting the same field on each surface. It is believed that the flat bottoms appearing in the original conical etch pits as the result of the thermal treatment (Figs. II-3(a-b)) occur because of a change in the direction of the dislocation. The subsequently re-etched surface (Fig. II-3(c)) supports this hypothesis, since there is a significant change in the position of the pits but not in their number.

The relative thermal etch rates of the principal low-index planes were examined in the light of the bonding configuration of the surface atoms. This work has been concluded and is being prepared for publication.

Mary C. Lavine
H. C. Gatos

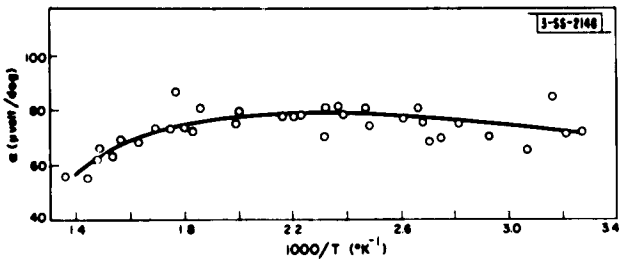

Fig. II-4. Seebeck coefficient vs reciprocal temperature for sample A, $PrO_{1.5239}$.

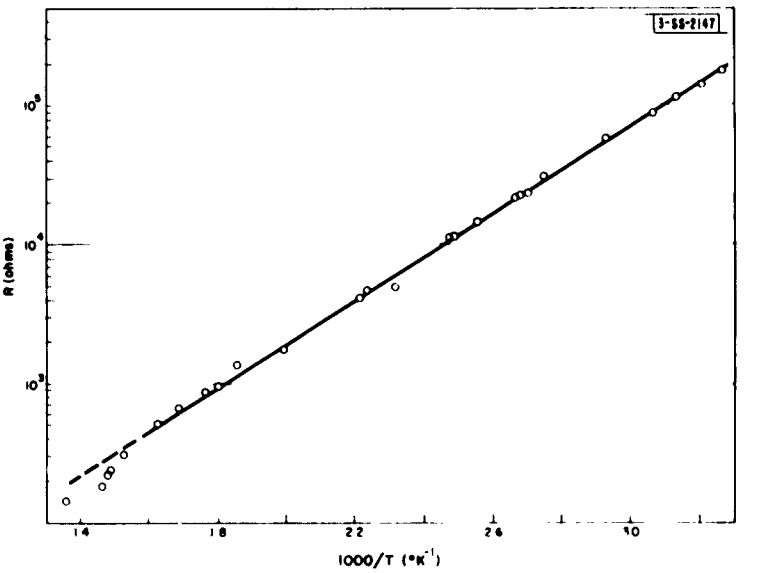

Fig. II-5. Resistance vs reciprocal temperature for sample A, $PrO_{1.5239}$.

4. Surface Bonding Characteristics of III-V Compounds

Many pronounced differences in chemical, structural and electrical properties between the A{111} and B{$\bar{1}\bar{1}\bar{1}$} surfaces of $A^{III}B^{V}$ compounds have been attributed to the bonding characteristics of the A and B surface atoms.[2-4] An attempt to assess quantitatively the strain associated with the distortion of the sp^3 bonding configuration of the A{111} surface atoms was made by studying the spontaneous bending of very thin single crystals of InSb.

If the thickness t of the thin single crystal is much less than its length or width, and assuming that the bending lies in the elastic range, it can be shown that the radius of curvature R is

$$R = \left(\frac{Et^3}{24nB_s f}\right)^{1/2} , \qquad (1)$$

where E is Young's modulus for the crystal, B_s is the bond energy per sp^3 bond, f is the fraction of the bond energy manifested in the distortion of the bonding configuration of the surface atoms and n is the number of distorted bonds per square centimeter of surface.

A single-crystal specimen of InSb 7.9 ± 0.4 microns thick, 2 cm long and 0.2 cm wide was carefully prepared, and its spontaneous radius of curvature was measured on a metallograph. A value of R equal to 82.6 ± 5 cm was obtained. Using this value in Eq. (1), f was calculated as 3.5×10^{-7}.

Measurements of radii of curvature for various sample thicknesses are currently being made to confirm the value of f. This work, coupled with annealing studies, should lead to further insight into the nature of surface bond distortion in $A^{III}B^{V}$ compounds.

R. E. Hanneman
Mary C. Finn
H. C. Gatos

B. PROPERTIES OF PrO_x AND SnO_2

1. Seebeck Coefficient and Resistance of PrO_x Single Crystals

Measurements of the Seebeck coefficient α and resistance R of a single-crystal sample of $PrO_{1.5239}$ (sample A), reported in part in the last quarterly progress report, were completed and are shown in Figs. II-4 and II-5. By using a Fluke electronic precision potentiometer and by careful shielding of the sample and lead wires, it was possible to extend the range of α measurements beyond the 5-megohm sample resistance. Data obtained with a second crystal (sample B) of PrO_x, $1.5 < x < 1.52$, having the same physical dimensions as sample A, are shown in Figs. II-6 and II-7.

As expected, the sample more nearly approaching the Pr_2O_3 stoichiometry (i.e., sample B) exhibits both a higher resistance and a greater Seebeck coefficient. The activation energy for electronic conduction also increased, from 0.310 to 0.562 ev. Further measurements with stoichiometries in the range $1.5 < x < 1.52$ are planned.

J. M. Honig
A. A. Cella

2. Seebeck Coefficient and Resistivity of SnO_2

Measurements of the Seebeck coefficient α and resistance R of single-crystal SnO_2 have been started; the method of preparation and properties of the undoped specimens were detailed in the last quarterly progress report. By momentary immersion of the SnO_2 needles in molten

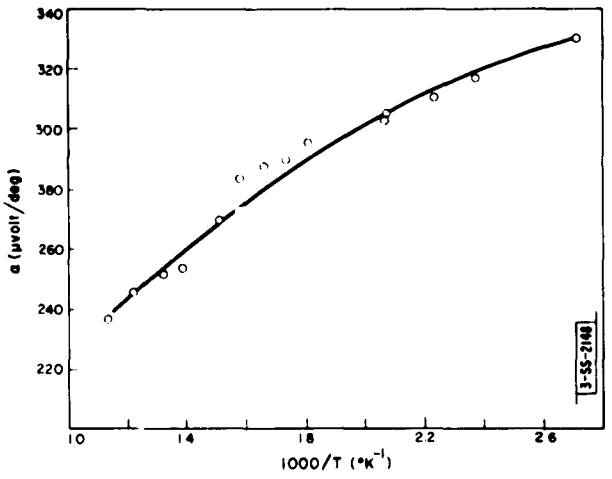

Fig. II-6. Seebeck coefficient vs reciprocal temperature for sample B.

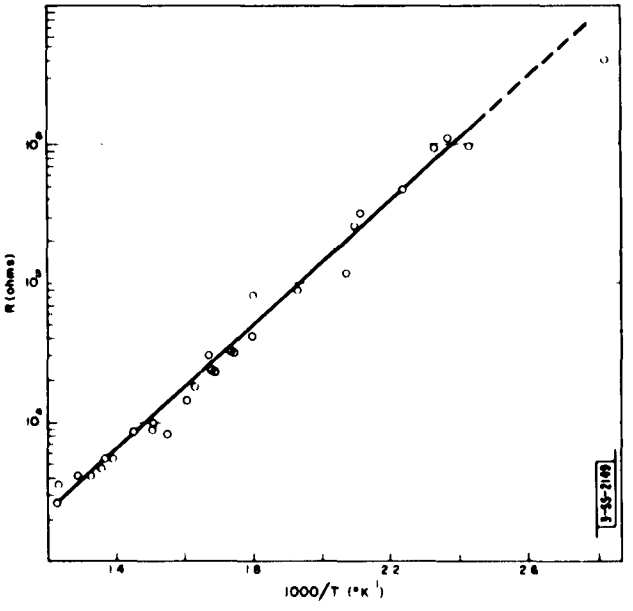

Fig. II-7. Resistance vs reciprocal temperature for sample B.

silver, the ends became coated with a thick deposit of silver to which electrical connections could be welded. Measurements were carried out in air since it had been established that the sample composition remained invariant on heating or cooling. The preliminary results of two runs on one sample are exhibited in Figs. II-8 and II-9.

The log R vs 1/T curve of Fig. II-9 exhibits a flat region which presumably characterizes the electrical properties of SnO_2 in the extrinsic exhaustion region. In the high temperature region R decreases exponentially with increasing T; presumably, the conduction is intrinsic, with an activation energy of 1.44 ev. In run 2, two- and four-probe resistance measurements (R_2 and R_4) were carried out simultaneously; comparison of the closed circles and squares in Fig. II-9 shows that the intrinsic activation energy is not appreciably affected by contact resistance. In the intrinsic region, $R_2/R_4 \approx 2.4$; the ratio calculated from measured geometric factors is 2.1. The negative Seebeck coefficient (Fig. II-8) exhibits a peculiar dip in the transition between extrinsic and intrinsic characteristics. Further measurements are planned.

J. M. Honig
A. A. Cella
T. B. Reed

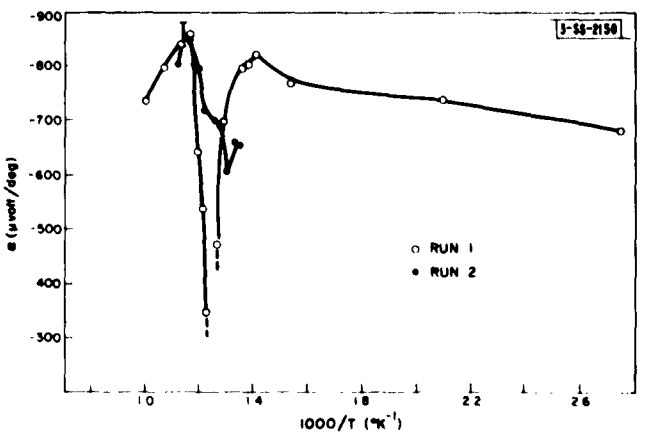

Fig. II-8. Seebeck coefficient vs reciprocal temperature for undoped SnO_2.

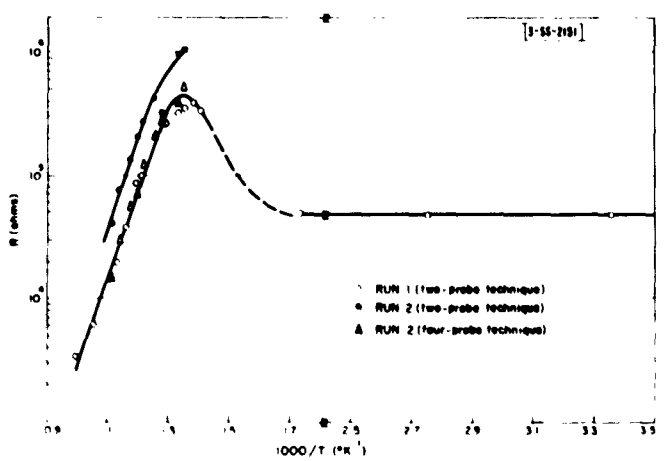

Fig. II-9. Resistance vs reciprocal temperature for undoped SnO_2.

3. Magnetic Susceptibility of Praseodymium Oxide

The vibrating-sample magnetometer is now operable from liquid helium to room temperature. Measurements made on a hexagonal crystal of $PrO_{1.500}$ gave an a-axis moment of 3.611 Bohr magnetons, which is in very good accord with theory. Attempts are now under way to prepare the $PrO_{1.500}$ in cubic form by means of a low-temperature hydrogen reduction of a higher oxide.

S. Kern

C. ANALYSIS OF MATERIALS

1. A Table of Mass Spectrographic Lines Grouped by Element

A table has been compiled which lists the lines observable by RF spark ionization of inorganic solids in a Mattauch-Herzog type double-focusing mass spectrograph. The table is arranged by element, and for each element the lines are listed in order of increasing apparent mass. The table records lines for all known naturally occurring isotopes, lines for ions with charge of +1 through +9, lines for multiatomic clusters containing from 1 to 10 atoms and lines due to eight of the more frequently occurring charge-exchange collisions. For each of these entries, the table gives the isotope and element identification, a coded explanation of the line formation, the apparent mass and the square root of the apparent mass to eight significant figures (when the mass is known to this accuracy), and the relative abundance.

The table has been used in this laboratory for the past six months and, for the identification of mass spectrum lines, has proved to be a very useful complement to the Table of Atomic Masses compiled by R. L. Heath.[5] The Heath table presents the lines of all elements in one continuous list going from the lowest to the highest apparent mass and is very useful for making tentative line identifications. The table compiled in this laboratory, being arranged by element, has the advantage of making the confirmation or rejection of tentative identifications much more convenient and also of aiding in the rapid identification of all lines due to the major elements of the sample.

The table, which was generated on the IBM 7090 computer, will be published in a forthcoming technical report to make it available for distribution to other workers in the field of solid mass spectrography.

E. B. Owens
Ann M. Sherman

2. Polarographic Analysis of HgTe-CdTe Alloys

In an effort to eliminate the erratic behavior occurring in the polarographic analysis of HgTe-CdTe alloys, the use of a tapered capillary was investigated. Cooke, Kelley and Fisher[6] recommend using a tapered capillary to reduce the effects causing capillary noise. It was found that a sharp taper was necessary to obtain a suitably slow drop time (~3 sec). With this arrangement the carrier waves were much smoother than before and without erratic peaks. Preliminary results on HgTe-CdTe alloys suggest that, because of the reduced oscillations, it may be possible to analyze alloys containing less than 10 mole per cent CdTe without prior removal of mercury. This possibility is being investigated.

M. C. Gardels
J. C. Cornwell

REFERENCES

1. Quarterly Progress Report on Solid State Research [U], Lincoln Laboratory, M.I.T. (15 October 1961), p.13, ASTIA 266878, H-360.

2. H.C. Gatos and M.C. Lavine, J. Electrochem. Soc. 107, 427 (1960).

3. H.C. Gatos, M.C. Lavine and E.P. Warekois, J. Electrochem. Soc. 108, 645 (1961).

4. M.C. Lavine, H.C. Gatos and M.C. Finn, J. Electrochem. Soc. 108, 974 (1961).

5. Table of Atomic Masses, compiled by R.L. Heath, edited by J.W. Guthrie, Sandia Corporation Monograph SCR-245, TID-4500 (16th edition) (February 1961).

6. W.D. Cooke, M.T. Kelley and D.J. Fisher, Anal. Chem. 33, 1209 (1961).

III. MATERIALS RESEARCH

A. STOICHIOMETRY OF $Cd_xHg_{1-x}Te$ ALLOYS

Preparation of $Cd_xHg_{1-x}Te$ alloys with electron mobilities exceeding 5×10^5 cm^2/volt-sec at 77°K has been reported previously.[1] Deviations from stoichiometry in alloys containing up to 30 mol per cent CdTe are being investigated in an attempt to prepare materials with still higher mobilities and with carrier concentrations suitable for band parameter studies and electronic applications. In initial experiments samples grown by the Bridgman technique have been annealed at 400°C in evacuated ampoules or in the presence of mercury vapor, and their Hall coefficients have been measured at 300°, 77° and 4.2°K. A consistent qualitative explanation of the results can be given if it is assumed, by analogy with $HgTe_xSe_{1-x}$ alloys, that samples containing excess Te atoms are p-type (contain excess acceptors) and that those containing excess metal atoms are n-type (contain excess donors). Then the observed changes in Hall coefficients on annealing can be attributed to changes in the metal/Te ratio. As expected, vacuum annealing tends to make samples p-type by removing mercury and thus decreasing the metal/Te ratio; annealing in mercury vapor tends to make them n-type by increasing the ratio. The changes are reversible.

For most of the samples investigated so far, the concentration of excess acceptors or donors associated with stoichiometric deviations cannot be determined from the measured Hall coefficients. The principal exceptions are vacuum-annealed samples containing less than about 8 mol per cent CdTe. These samples have negative Hall coefficients at 300° and 77°K, but at 4.2°K they have positive Hall coefficients which correspond to hole concentrations of about 5×10^{18} cm^{-3} if a one-carrier model is assumed. These hole concentrations are probably about equal to the excess acceptor concentrations resulting from metal deficiencies. Most of the as-grown and mercury-annealed samples in the same composition range have negative Hall coefficients at all three temperatures. The Hall coefficient passes through a maximum as the temperature is decreased below 300°K, and the Hall mobilities at 77° and 4.2°K are less than 10^4 cm^2/volt-sec. These data indicate that the samples are p-type but contain fewer excess acceptors than the vacuum-annealed samples. Their Hall coefficients are negative even at 4.2°K because of a high ratio (~100) of electron-to-hole mobility and high intrinsic carrier concentrations. Since they are in the mixed conduction range at all temperatures, their Hall coefficients cannot be used to determine their excess acceptor concentrations. (The intrinsic carrier concentrations at 4.2°K in these samples appear to be too high to be consistent with a finite energy gap between the valence and conduction bands. Therefore, the overlapping band model proposed previously[2] for HgSe and $HgSe_{0.5}Te_{0.5}$ alloys also seems to apply to HgTe and the low-cadmium alloys.)

For the high-mobility samples reported previously, in all of which the CdTe content exceeds 13 mol per cent, the Hall coefficients are negative at all three temperatures and increase with decreasing temperature. These samples are apparently n-type or so weakly p-type that a single-carrier model is applicable at all temperatures, with $n = -1/R_H e$. The electron concentrations measured at 4.2°K are of the order of 10^{15} cm^{-3}. It cannot be assumed that these values correspond to excess donor concentrations associated with an excess of metal atoms, since they are low enough to be due to intrinsic carriers or to foreign impurities.

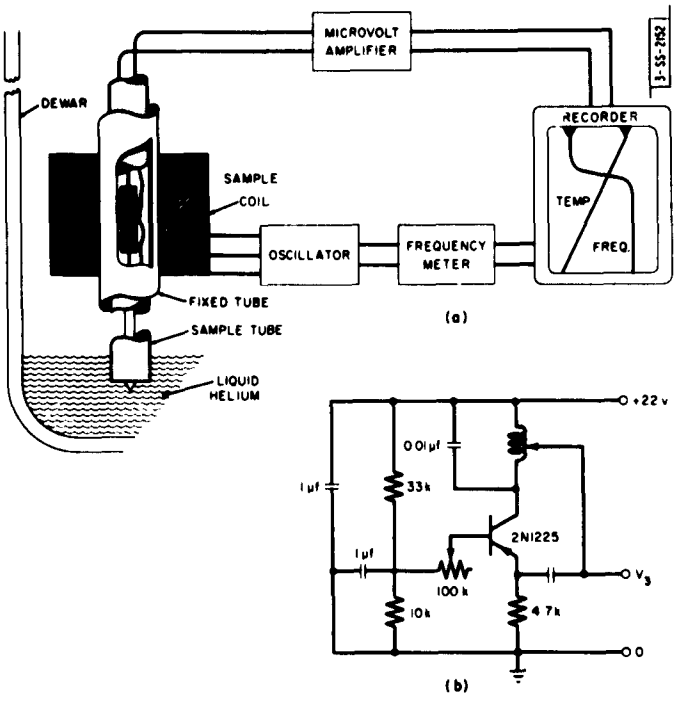

Fig. III-1. (a) Schematic diagram of transition temperature apparatus; (b) schematic of transistorized oscillator in (a).

Fig. III-2. Relative permeability vs temperature for Nb_3Sn-cored niobium wire.

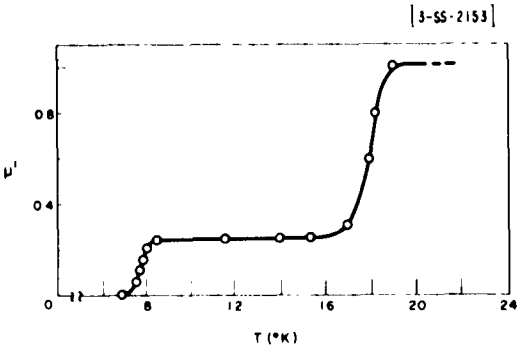

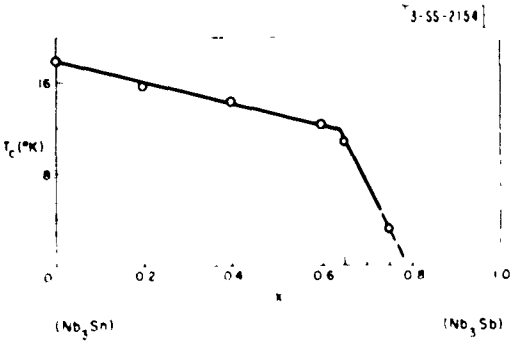

Fig. III-3. Superconducting transition temperatures for $Nb_3Sb_xSn_{1-x}$.

The data obtained so far indicate that under similar annealing conditions the metal/Te ratio in the $Cd_xHg_{1-x}Te$ alloys tends to increase with increasing cadmium content. They also indicate that because of mixed conduction the electron mobilities in low-cadmium alloys have not yet been measured. An attempt is being made to prepare n-type samples of these alloys by mercury annealing so that valid measurements can be made.

T. C. Harman
A. J. Strauss

B. SUPERCONDUCTING MATERIALS

1. Transition Temperature Apparatus

The relative permeability of a superconductor changes from zero in the superconducting state to approximately one in the normal state. An apparatus has been constructed for studying superconducting transitions by making continuous measurements of relative permeability as a function of temperature. Since the permeability does not depend on electrical continuity, this method is more suitable than a resistance method for measurements on inhomogeneous materials, powders and ingots.

A schematic diagram of the apparatus is shown in Fig. III-1(a). The sample is attached to one junction of a thermocouple (Au-Co vs Cu) and lowered into a measuring coil which forms part of the oscillator circuit shown in Fig. III-1(b). The frequency of oscillation (about 700 cps), which depends on the permeability of the sample, and the thermocouple voltage are recorded on a dual-channel recorder. The measuring coil is located in the gas region of a liquid helium dewar, and the cold junction of the thermocouple is immersed in the liquid helium. Over the range between 5° and 40°K, the sample temperature can be raised or lowered at rates as low as 0.1°/minute by adjusting the current through two hollow resistors, one above and one below the liquid helium level.

An example of the results obtained for inhomogeneous samples is given in Fig. III-2, which shows the data for a Nb_3Sn-cored niobium wire. The transition at 7.6°K is due to niobium, and the transition at 17.8°K is due to Nb_3Sn.

2. Pseudo-Binary Nb_3Sn-Nb_3Sb System

In view of the fact that the compound Nb_3Sn has the highest superconducting transition temperature known, whereas the neighboring compound Nb_3Sb (which also has the β-tungsten structure) exhibits no superconductivity above 1.0°K, it was considered worthwhile to study the pseudo-binary system $Nb_3Sb_xSn_{1-x}$. The ternary materials were prepared by sintering powders of the elements at 1000°C for 16 hours. X-ray powder patterns of these materials exhibited only β-tungsten lines, and no unreacted elements were detected. The superconducting transition temperatures for the compositions prepared thus far are shown in Fig. III-3. The alloy $Nb_3Sn_{0.25}Sb_{0.75}$ exhibited only the end of a superconducting transition at 4.2°K, the lowest temperature attainable in the apparatus described above. Thus the transition temperature indicated for this composition in Fig. III-3 represents an approximation.

T. B. Reed
H. C. Gatos
W. J. LaFleur

3. Nb_3In

The compounds Nb_3Ga, Nb_3Al and Nb_3Sn, all of which have the β-tungsten structure, are superconductors with high transition temperatures. Previous attempts here and in other laboratories to synthesize the chemically related compound Nb_3In by conventional powder metallurgy and arc-melting techniques have been unsuccessful. This compound has now been prepared by heating powdered niobium and indium in stoichiometric proportions to 1200°C under high pressure (approximately 45,000 bars). X-ray powder patterns show that the compound has the β-tungsten structure with lattice parameter $a_o = 5.303\text{Å}$. The powder patterns also reveal the presence of some unreacted niobium and indium. The lattice parameters of Nb_3Al, Nb_3Ga and Nb_3In reflect the variation in the metallic radius of the Group III elements, as shown in Fig. III-4(a) and (b).

The superconducting transition temperature of Nb_3In was found to be 9.2°K by permeability measurements. Typical results obtained with two different samples are shown in Fig. III-5. Repeated measurements on these two samples gave transition temperatures (corresponding to a relative permeability of 0.5) of 9.16 ± 0.1°K and 9.28 ± 0.06°K, respectively. As shown in Fig. III-4(c), the transition temperatures of Nb_3Al,[3] Nb_3Ga,[3] and Nb_3In decrease monotonically with increasing atomic number of the Group III element.

M. D. Banus
T. B. Reed
H. C. Gatos
Mary C. Lavine
J. A. Kafalas

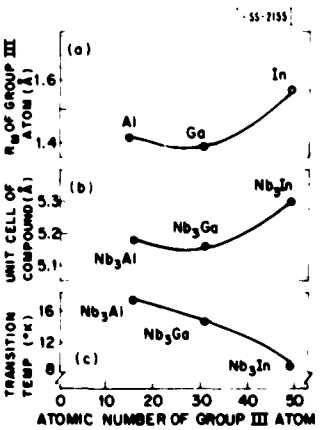

Fig. III-4. (a) Metallic radii of Al, Ga and In; (b) lattice parameters of Nb_3Al, Nb_3Ga and Nb_3In; (c) superconducting transition temperatures of Nb_3Al, Nb_3Ga and Nb_3In.

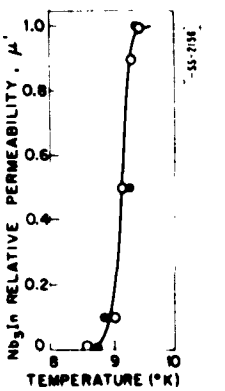

Fig. III-5. Relative permeability vs temperature for two samples of Nb_3In.

C. VAPOR-PHASE GROWTH OF GERMANIUM AND SILICON CRYSTALS

We are investigating the possibility of obtaining large crystals of Ge or Si uniformly doped with S, Se, or Te by using the Group VI elements as carriers for vapor-phase growth. Such crystals are desired for optical studies of the energy levels of these impurities. In preliminary experiments large-grained deposits about 1 cm in their largest dimension have been obtained by slowly pulling an evacuated quartz ampoule containing the semiconductor charge and a few milligrams of the Group VI element through a temperature gradient in a vertical tube furnace. A somewhat similar method has been used by Piper and Polich[4] for the vapor-phase growth of II-VI compounds. The electrical properties of the germanium and silicon deposits have not yet been measured.

S. Fischler

D. PREPARATION AND STRUCTURE OF PRASEODYMIUM SUBOXIDE

Although the divalent compounds PrS, PrSe and PrTe are known, the lowest oxide of praseodymium which has been reported is $PrO_{1.5}$. A gray oxide of slightly lower valency has been prepared by reduction of Pr_6O_{11} with circulating hydrogen under stringent drying conditions above 600°C. On reheating the reaction product in vacuum in the presence of traces of moisture, the sample gained mass and was converted to a material with the green-white color characteristic of $PrO_{1.5}$. If the latter material is assumed to be $PrO_{1.5}$, the mass change leads to the formula PrO_x, with $1.47 < x < 1.495$, for the gray oxide.

X-ray powder patterns of a sample with composition $PrO_{1.47}$ were taken over the range 25° to 1000°C at temperature. These patterns showed sharp lines out to very high orders which indexed to an FCC structure with a BCC superlattice. The FCC lattice parameter was $a_o = 5.575 \pm 0.005$Å and the BCC superlattice parameter was $a_1 = 11.15 \pm 0.01$Å at 25°C. Figure III-6 is a plot of a_o vs T and shows an unusual, abrupt contraction of a_o by 0.06Å (1.1 per cent), while maintaining the FCC structure, with increasing temperature at 750 ± 40°C. The nature of this contraction is being correlated to other property discontinuities in the oxide at this temperature. The thermal expansion coefficient α in the relation $a_T = a_o (1 + \alpha [T - 25])$ was found to be $\alpha = 1.2 \times 10^{-5}$/°C for $T \leq 710$°C and $\alpha = 1.7 \times 10^{-5}$/°C for $T \geq 790$°C.

R. E. Hanneman
J. M. Honig
A. A. Cella

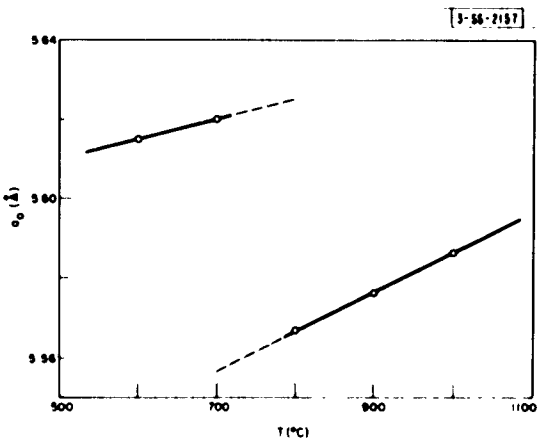

Fig. III-6. Lattice parameter (a_o) of $PrO_{1.47}$ as a function of temperature.

E. METAL WHISKERS

Iron whiskers up to 20 mm long and 0.3 mm in diameter have been prepared by the reduction of ferrous chloride with hydrogen. Generally these have a [100] or a [111] fiber axis, as reported in the literature. In several runs, however, whiskers with a [110] fiber axis, bounded by two (100) and four (443) planes have been obtained.

Chromium whiskers have been grown from a eutectic mixture of chromium and copper, but they are too small to be useful. A sublimation technique has been developed which has produced chromium whiskers 3 mm in length by 0.1 mm in diameter. The perfection of these crystals is being studied by both x-ray and electron diffraction.

T. P. Turnbull
M. Jane Button

F. HIGH PRESSURE RESEARCH

Pronounced hysteresis in the polymorphic transformation of various selenides under high pressure has been observed by measuring resistance as a function of pressure. Typical examples are shown in Figs. III-7 and III-8. For both HgSe and PbSe the high pressure phase is retained at pressures well below the transformation pressure. In the case of HgSe, it is possible to retain the high pressure phase at atmospheric pressure by cooling below room temperature. An x-ray investigation of the retained phase is in progress.

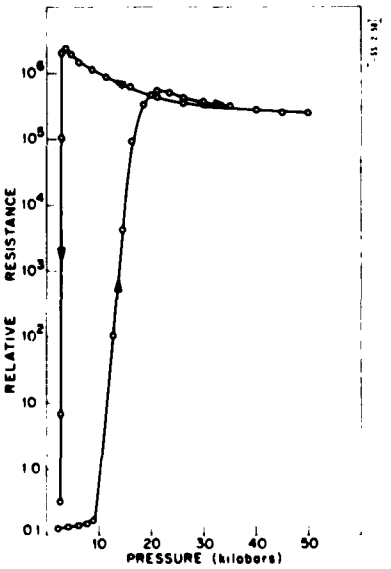

Fig. III-7. Resistance vs pressure for HgSe.

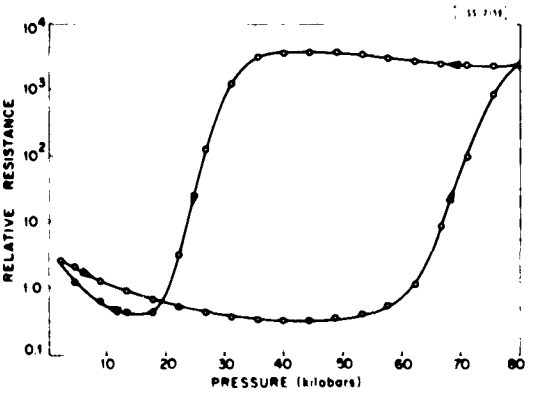

Fig. III-8. Resistance vs pressure for PbSe.

The polymorphism of InSb is being studied in detail as a function of pressure and temperature. The phase changes in this case are also being followed by means of resistance measurements. The InSb I → II transformation between 20° and 300°C recently reported by Jayaraman, et al.,[5] on the basis of volume change measurements has been essentially confirmed. The InSb high pressure phase is being studied by x-ray techniques. Preliminary measurements indicate that additional phases exist near the liquidus line of both I and II phases.

M. D. Banus H. C. Gatos
J. A. Kafalas Mary C. Lavine

REFERENCES

1. Quarterly Progress Report on Solid State Research [U], Lincoln Laboratory, M.I.T. (15 October 1961), p. 23, ASTIA 266878, H-360.
2. T.C. Harman and A. J. Strauss, J. Appl. Phys. 32, 2265 (1961).
3. E.A. Wood, V.B. Compton, B.T. Matthias and E. Corenzwit, Acta Cryst. 11, 604 (1958).
4. W.W. Piper and S. J. Polich, J. Appl. Phys. 32, 1278 (1961).
5. A. Jayaraman, R.C. Newton and G.C. Kennedy, Nature 191, 1288 (1961).

IV. BAND STRUCTURE OF SOLIDS

A. OPTICAL ABSORPTION IN SULFUR-DOPED SILICON

The optical absorptions seen in compensated and uncompensated sulfur-doped silicon[1] have been correlated with the excited states of neutral and singly ionized helium atoms embedded in a dielectric medium. The results will be submitted for publication in The Physical Review.

W. E. Krag
H. J. Zeiger

B. EXPERIMENTAL EVIDENCE FOR THE THIRD VALENCE BAND RESONANCE AND HEAVY HOLE BAND RESONANCE IN p-TYPE DIAMOND

Previous cyclotron resonance experiments in diamond[2] in which carriers were excited with a tungsten light source suggested that the 0.70 m_o line was due to the light hole and the 1.06 m_o line was due to the split off or third valence band.

The above has been confirmed by using the millimeter cyclotron resonance as the detector in an optical spectrometer. Holding the millimeter wave system on the low and high field resonances respectively, and sweeping the optical monochromator, yields acceptor binding energies. The difference in these levels ($\Delta \sim 0.006$ ev) is a measure of the spin-orbit splitting.

These data indicate that the heavy hole should have a mass of $\sim 2.12\, m_o$ and this has been confirmed by experiments in a Bitter magnet with fields up to 68.8 kgauss.

Further experiments are in progress, and a detailed article is being submitted for publication in The Physical Review.

C. J. Rauch

C. GALVANOMAGNETIC EFFECTS IN n-TYPE GERMANIUM

Calculations of the galvanomagnetic effects in n-type germanium are under way. These calculations are to be done in a similar manner to those previously reported for n-type silicon.[3] The computer program for an IBM 7090 has been written and is now in the process of being checked out for several cases. The calculations are to be compared with the experimental data previously published by Bullis,[4] as well as with other types of data.[5]

W. E. Krag
M. Clare Brown

D. GALVANO-THERMOMAGNETIC EFFECTS IN DEGENERATE MATERIALS

The phenomenological equations previously developed[6] for degenerate materials with spherically symmetric bands, but arbitrary band shape, involved a set of transport integrals K_i and G_j. These have now been rewritten as functions of ϵ or k and parameters. For this purpose one must replace the reciprocal effective mass $1/m$ by $(1/\hbar^2 k)\,(d\epsilon/dk)$. Radcliffe[7] has shown that when deformation scattering due to acoustic modes predominates, the relaxation time is given by $\tau = \tau_1 k^{-2}(d\epsilon/dk)$. According to Barrie[8] the corresponding function for ionized impurity scattering is $\tau = \tau_2 k^2 (d\epsilon/dk)$. This suggests a general dependence of the form

$$\tau = \tau_o (k^2)^{r-1} (d\epsilon/dk) \quad ,$$

where r is a scattering parameter and τ_o is independent of ϵ or k but may vary parametrically

with quantities such as temperature and dielectric constant. With the definitions

$$\beta = ZeH_z\tau_o(\underset{\sim}{k}T)^2/\hbar c$$

$$g = (c/3\pi^2)\,(Ze\beta/H_z) = 4e^2(\underset{\sim}{k}T)^2\tau_o/3h^2 \quad ,$$

the transport integrals of interest become

$$K_i = (\underset{\sim}{k}T)^{i-1}\,(g/e^2)\,I_i$$

$$G_j = (\underset{\sim}{k}T)^{j-1}\,(g/e^2)\,(\beta/ZeH_z)\,J_j \quad ,$$

where

$$I_i = \int_o^\infty \frac{x^{i-1}k^{2r}(\partial x/\partial k)^2\, e^{x-\eta}}{(1+e^{x-\eta})^2\,[1+\beta^2(k^2)^{2r-3}\,(\partial x/\partial k)^4]}\,dx \quad ,$$

$$J_j = \int_o^\infty \frac{x^{j-1}k^{4r-3}(\partial x/\partial k)^4\, e^{x-\eta}}{(1+e^{x-\eta})^2\,[1+\beta^2(k^2)^{2r-3}\,(\partial x/\partial k)^4]}\,dx$$

and $x \equiv \epsilon/\underset{\sim}{k}T$, $\eta \equiv \mu_B/\underset{\sim}{k}T$.

Finally, denoting the lattice thermal conductivity as κ_L and writing $J_Q^\lambda = J_{Q'}^\lambda - \kappa_\lambda \nabla_\lambda T$ ($\lambda = x, y$) the phenomenological equations read

$$\begin{bmatrix} \frac{J^x}{g} \\ \frac{J^y}{g} \\ \frac{ZeJ_Q^x}{g\underset{\sim}{k}T} \\ \frac{ZeJ_Q^y}{g\underset{\sim}{k}T} \end{bmatrix} = \begin{bmatrix} I_1 & \beta J_1 & \frac{\underset{\sim}{k}}{Ze}(I_1\eta - I_2) & \frac{\underset{\sim}{k}}{Ze}\beta(J_1\eta - J_2) \\ -\beta J_1 & I_1 & \frac{-\underset{\sim}{k}\beta}{Ze}(J_1\eta - J_2) & \frac{\underset{\sim}{k}}{Ze}(I_1\eta - I_2) \\ I_2 & \beta J_2 & \frac{\underset{\sim}{k}}{Ze}(I_2\eta - I_3) - \frac{Ze}{g\underset{\sim}{k}T}\kappa_L & \frac{\underset{\sim}{k}\beta}{Ze}(J_2\eta - J_3) \\ -\beta J_2 & I_2 & \frac{-\underset{\sim}{k}\beta}{Ze}(J_2\eta - J_3) & \frac{\underset{\sim}{k}}{Ze}(I_2\eta - I_3) - \frac{Ze}{g\underset{\sim}{k}T}\kappa_L \end{bmatrix} \begin{bmatrix} \nabla_x(-\frac{\zeta}{Ze}) \\ \nabla_y(-\frac{\zeta}{Ze}) \\ \nabla_x T \\ \nabla_y T \end{bmatrix} .$$

Accordingly, one can write expressions for various transport coefficients: for the isothermal conductivity in a magnetic field,

$$\sigma_I(H_z) \equiv J^x/\nabla_x(-\tfrac{\zeta}{Ze})\Big]_{\nabla_x T=\nabla_y T=J^y=0} = g(I_1^2 + \beta^2 J_1^2)/I_1$$

for the isothermal Hall coefficient,

$$\mathcal{R}_I(H_z) \equiv \nabla_y(-\zeta/Ze)/H_z J^x\Big]_{\nabla_x T=\nabla_y T=J^y=0} = (\beta/gH_z)\,J_1/(I_1^2 + \beta^2 J_1^2)$$

for the isothermal heat conductivity in a magnetic field,

$$\kappa_I(H_z) \equiv -J_Q^x/\nabla_x T\Big]_{J^x=J^y=\nabla_y T=0} = \kappa_L + \frac{k^2 T}{e^2}\, g \left\{\frac{I_3 I_1^2 - I_1 I_2^2 + \beta^2(J_1^2 I_3 - 2J_1 J_2 I_2 + I_1 J_2^2)}{I_1^2 + \beta^2 J_1^2}\right\}$$

for the isothermal Ettingshausen-Nernst coefficient,

$$P_I \equiv \nabla_x(-\zeta/Ze)/\nabla_x T\Big]_{J^x=J^y=\nabla_y T=0} = \frac{k}{Ze}\left\{\frac{I_1 I_2 + \beta^2 J_1 J_2}{I_1^2 + \beta^2 J_1^2} - \eta\right\}$$

for the isothermal transverse Nernst coefficient,

$$\mathcal{N}_I(t) \equiv \nabla_y(-\zeta/Ze)/H_z\nabla_x T\Big]_{J^x=J_Q^x=\nabla_y T=0} = \frac{k\beta}{ZeH_z}\left\{\frac{J_1 I_2 - J_2 I_1}{I_1^2 + \beta^2 J_1^2}\right\}$$

for the Righi-Leduc coefficient,

$$\mathcal{N} = \nabla_y T/H_z\nabla_x T\Big]_{J^y=J^x=J_Q^x=0} = \frac{\beta g k^2 T}{e^2 H_z \kappa_I}\left\{\frac{J_1 I_2^2 - 2I_1 I_2 J_2 + I_1^2 J_3 - \beta^2(J_1 J_2^2 - J_1^2 J_3)}{I_1^2 + \beta^2 J_1^2}\right\} .$$

Numerical calculations of the requisite integrals I_i and J_j are in progress.

T. C. Harman
J. M. Honig

E. LANDAU LEVELS FOR BLOCH ELECTRONS IN A MAGNETIC FIELD

An extension has been made of the classical result for the cyclotron frequency and hence for the energy levels of a Bloch electron in a magnetic field.

Earlier work[9] has shown that, for nondegenerate bands, a one-band momentum space Hamiltonian $\mathcal{H}(\vec{\kappa})$ can be obtained as an expansion in powers of the magnetic field, the first term of which is the energy function $\mathcal{E}(\vec{\kappa})$. Here $\vec{\kappa}$ is the operator $\vec{k} + (e/c)\,\vec{A}(i\nabla_k)$, where $\vec{A}$ is the vector potential, and $\mathcal{H}(\vec{\kappa})$ is obtained from $\mathcal{H}(\vec{k})$ by replacing $\vec{k}$ by $\vec{\kappa}$ in a completely symmetric way.[9] Assuming we have an eigenfunction ψ belonging to an energy $\mathcal{E}$, if we find an operator G such that

$$[\mathcal{H}(\vec{\kappa}),\ G] = G\omega(\mathcal{H}, k_z) \quad , \tag{1}$$

where k_z is the component of $\vec{k}$ in the direction of the magnetic field, then $G\psi$ will be an eigenfunction of $\mathcal{H}$ with energy $\mathcal{E} + \omega(\mathcal{E}, k_z)$. If we now assume that G is a symmetrized function of $\vec{\kappa}$, we can symmetrize both sides of Eq. (1) by the methods of Ref. 9. It is then possible to obtain $G(\vec{k})$ and ω to any order in the magnetic field. The result for the levels can be put in the form of Onsager's relation

$$A(\mathcal{E}_n) = 4\pi\hbar[n + \gamma(\mathcal{E}_n)] \quad , \tag{2}$$

where A is the area enclosed by the cyclotron orbit, $\hbar = eH/2\hbar c$, and γ is obtained as an expansion in powers of $\hbar$.

If our effective Hamiltonian for a nondegenerate band is given by

$$\mathcal{H}(\vec{k}) = \mathcal{E}(\vec{k}) + \mathcal{H}_1(\vec{k})\,\hbar + \mathcal{H}_2(\vec{k})\,\hbar^2 \quad , \tag{3}$$

then to first order in h

$$\gamma = \frac{1}{2} + \oint \frac{d\lambda}{4\pi v} \varkappa_1 + h \oint \frac{d\lambda}{4\pi v} \varkappa_2 + h \frac{\partial}{\partial \mathcal{E}} \oint \frac{d\lambda}{4\pi v} \left[\frac{1}{6} \left(\mathcal{E}_{xx}\mathcal{E}_{yy} - \mathcal{E}_{xy}^2\right) - \frac{1}{2} \varkappa_1^2\right], \quad (4)$$

where the line integral is over the classical orbit, and $v = [\mathcal{E}_x^2 + \mathcal{E}_y^2]^{1/2}$. This result holds for closed orbits which enclose a single-band extremum for constant k_z, and breaks down near saddle-point extrema where the orbit may, for example, form a figure eight. This case is being investigated. The expansion is undoubtedly asymptotic since effects such as banding,[10] which depend exponentially on 1/H, are not included. A more general form of G can be used to discuss open orbits.

From Eq. (4) for γ, it is possible to obtain a derivation of the deHaas-vanAlphen effect somewhat similar to that of Lifshitz and Kosevich,[11] but which gives the normal susceptibility correctly.

Laura M. Roth

F. GENERAL STATISTICAL MECHANICAL THEORY OF RESONANCE

A general model of magnetic and electronic resonance consists of a driven system interacting with a heat bath. Starting from the Liouville equation for the density operator for the combined system we derive a Boltzmann-like equation for the density operator of the system of interest only, which describes its resonance. In this derivation the unsatisfactory statistical assumption of repeated random phases is eliminated. The only statistical assumption made concerns the state of the total system just prior to the application of the time-varying driving field. No further assumptions are made about the heat bath. The theory is valid for arbitrary strengths of the driving field; thus the phenomenon of saturation is also described. For the linear response of the system, the terms describing the correct "relaxation distribution" are obtained. Formal expressions describing the relaxation to all orders in the interaction of the system with the heat bath are obtained. This method has been applied to the phenomena of magnetic and cyclotron resonance.

P. N. Argyres

REFERENCES

1. Quarterly Progress Report on Solid State Research [U], Lincoln Laboratory, M.I.T. (15 October 1961), p.37, ASTIA 266878, H-360.
2. C.J. Rauch, Phys. Rev. Letters 7, 83 (1961).
3. W. Krag, Phys. Rev. 118, 435 (1960).
4. W.M. Bullis, Phys. Rev. 109, 292 (1958).
5. W.M. Bullis and W. Krag, Phys. Rev. 101, 580 (1956); C. Goldberg, Phys. Rev. 109, 331 (1958).
6. Quarterly Progress Report on Solid State Research [U], Lincoln Laboratory, M.I.T. (15 October 1961), p.31.
7. J.M. Radcliffe, Proc. Phys. Soc. (London) A68, 675 (1955).
8. R. Barrie, Proc. Phys. Soc. (London) B69, 553 (1956).
9. L.M. Roth, "Theory of Bloch Electrons in a Magnetic Field," to be published in Phys. Chem. Solids.
10. Quarterly Progress Report on Solid State Research [U], Lincoln Laboratory, M.I.T. (15 October 1961), p.33.
11. Lifshitz and Kosevich, Soviet Phys. J.E.T.P. 2, 636 (1956).

V. MICROWAVE AND MAGNETIC PROPERTIES OF SOLIDS

A. MILLIMETER WAVE PROGRAM

1. Antiferromagnetic Resonance in Powders

In the past, antiferromagnetic resonance experiments have been confined to single-crystal specimens. In many cases it is difficult to grow single crystals of sufficient purity to obtain significant data since small amounts of impurity may alter the internal fields markedly. For uniaxial antiferromagnetics it is possible, however, to obtain useful data from powdered materials, which can usually be prepared in a highly pure state. In the case of powdered samples, an absorption edge rather than a resonance line is observed as the magnetic field is increased. This can be briefly explained as follows: the applied magnetic field required for resonance for each individual crystallite of the powder increases with the angle which the axis of symmetry of the crystallite makes with the applied magnetic field and is a minimum when this angle is zero.

Figure V-1 shows the measured absorption edge in powdered $MnTiO_3$ at various frequencies as a function of applied magnetic field at 4.2°K. The position of the edge as a function of frequency behaves in accordance with the usual resonance equation for a uniaxial antiferromagnetic with the applied field along the c-axis. However, the exact point on the absorption edge which corresponds to the single-crystal resonance remains to be calculated. A theoretical analysis of the absorption edge to determine this point is in progress.

For zero applied field, the absorption is a function only of temperature and is independent of the orientation of the individual crystallites in the powder. It is therefore possible to measure zero-field resonance in the powder by observing the temperature at which the absorption is a maximum.

2. Antiferromagnetic Resonance in $MnTiO_3$

Additional measurements of antiferromagnetic resonance have been made on single-crystal and powdered $MnTiO_3$ samples as a function of both frequency and temperature.

Figure V-2 shows the variation of resonant frequency with applied magnetic field for two single-crystal samples C-1 and C-2 and a powder sample,* measured at 4.2°K. The zero-field resonances measured for samples C-1 and C-2 are 134 and 154 kMcps, respectively. This large variation is believed to be associated with impurities in the crystal. The powder sample, composed of very pure $MnTiO_3$, gave close agreement with single-crystal sample C-2. The value of the internal effective field $\sqrt{2H_E H_A}$ for the powder and single-crystal samples is 52 kgauss, and the g-value computed from the slope of the curve is close to 2.1.

The temperature at which zero-field resonance occurs was measured at frequencies from 84 to 153 kMcps. This was accomplished by observing the field required for resonance as the sample warmed up slowly from liquid helium temperature. A plot of the frequencies, normalized to unity at 4.2°K, vs normalized temperature is shown in Fig. V-3. The solid curve gives the Brillouin function for a spin of 5/2. The best fit to this curve requires that the single-crystal samples C-1 and C-2 have Néel temperatures of 66° and 64.5°K, and the powder sample, a Néel temperature of 63°K. Measurements of the Néel temperature by DC susceptibility measurements are now in progress.

G. S. Heller
J. J. Stickler

*Prepared by Dr. Aaron Wold, Group 53.

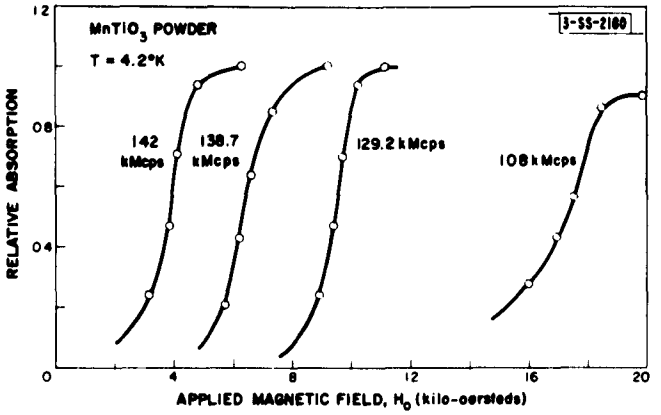

Fig. V-1. Absorption edges in $MnTiO_3$ powder.

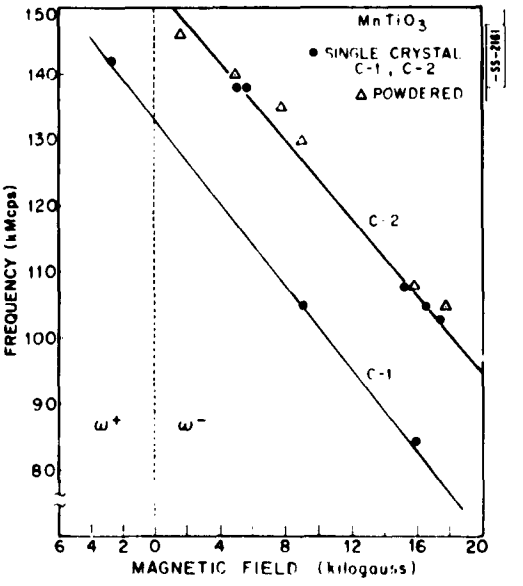

Fig. V-2. Resonant frequency vs applied magnetic field for two different single crystals and a powdered sample of MnTiO3. The ω^+ branch has been reflected at zero magnetic field.

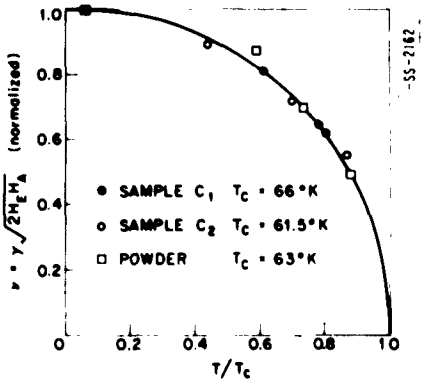

Fig. V-3. Normalized internal field vs normalized temperature. The solid line represents a Brillouin function for S = 5/2.

3. Temperature Dependence of the Internal Fields in Cr_2O_3

In order to obtain the temperature dependence of $\sqrt{2H_EH_A}$ from resonance data for a uniaxial crystal when the applied field H is along the c-axis, knowledge of the ratio of the parallel-to-perpendicular susceptibilities, $\alpha = \chi_{||}/\chi_{\perp}$, as a function of temperature is needed. The value of $\sqrt{2H_EH_A}$ is then computed from the resonance equation

$$\omega/\gamma = \sqrt{2H_EH_A + (\frac{\alpha H}{2})^2} \pm H(1 - \alpha/2) \quad .$$

When resonance data are taken with the applied field perpendicular to the c-axis, the appropriate resonance equation

$$\omega/\gamma = \sqrt{2H_EH_A + H^2}$$

is seen to be independent of α. Consequently, accompanying DC susceptibility measurements are not needed.

Measurements of $\sqrt{2H_EH_A}$ as a function of temperature by this means have been initiated.

J. B. Thaxter
G. S. Heller

4. Quantum Effects in Silicon at 2 mm

Further measurement of cyclotron resonance in p-type silicon at 4.2°K has been made in an attempt to observe any additional quantum resonances for a magnetic field applied along the [111] crystal direction. A cylindrical TE_{113} cavity (5/32 inch diameter), having a 0.038-inch hole midway between the end walls for light excitation, was constructed for this test. The silicon sample, in the form of a rectangular wafer (dimensions 0.100 × 0.040 × 0.013 inch, the narrow dimension along the [110] direction), was inserted in the cavity with the (110) plane of the sample normal to the direction of light illumination. The applied magnetic field was oriented along the [111] crystal direction by rotating the magnet in the (110) crystal plane.

Several additional quantum resonances not previously reported were observed. One quantum resonance with an effective mass close to 0.126 was observed when the light illumination was reduced to minimize heating effects. Correlation between the measured effective masses and the theoretical expected values is now in progress.

J. J. Stickler
G. S. Heller

5. Analysis of Quantum Effects in Ge and Si

We have been able to obtain a fairly good fit of the observed spectrum lines in the Ge quantum effect spectrum for H along [111], with the exception of four fairly weak experimental lines. The parameters for the best fit are $\gamma_1 = 14.12$, $\gamma_2 = 4.63$, $\gamma_3 = 6.06$, $\kappa = 3.92$. Possible explanations of the extra lines are being considered. Among these are carriers in other bands, or resonances associated with pockets at the ends of the constant energy surfaces for the heavy mass hole band.

A number of new experimental lines that have been found in the data for quantum effects in Si (see Sec. V-A-4) lend further support to a tentative theoretical fit of the Si spectrum. Figure V-4 shows a comparison of the experimental spectrum in Si, together with our best fit to date. Figures V-5 and V-6 show the energy level diagrams for Ge and Si.

H. J. Zeiger
G. W. Catuna

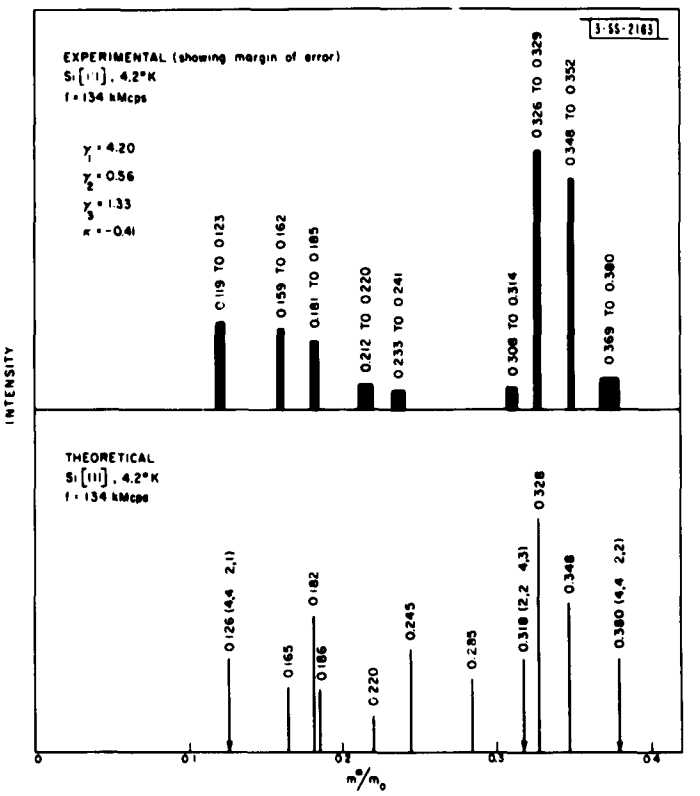

Fig. V-4. Comparison of theoretical and experimental spectra of quantum effect lines in Si, with H along [111]. The arrows indicate positions of $\Delta n = \pm 2$, $\Delta n = \pm 3$ transitions. The remaining $\Delta n = \pm 1$ theoretical line intensities have been calculated.

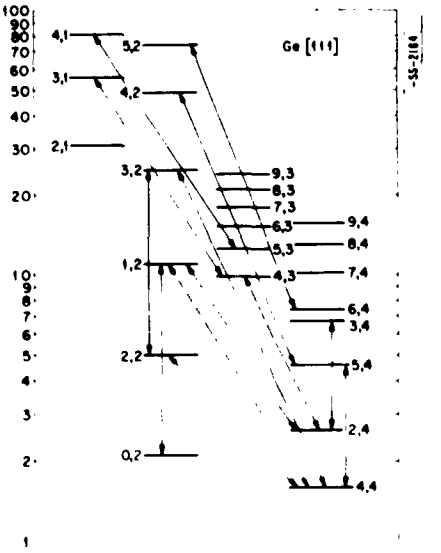

Fig. V-5. Low-lying energy levels of holes in the valence bands of Ge. The full lines show prominent transitions observed in the spectra. The dotted lines show $\Delta n = \pm 2$, $\Delta n = \pm 3$ transitions observed.

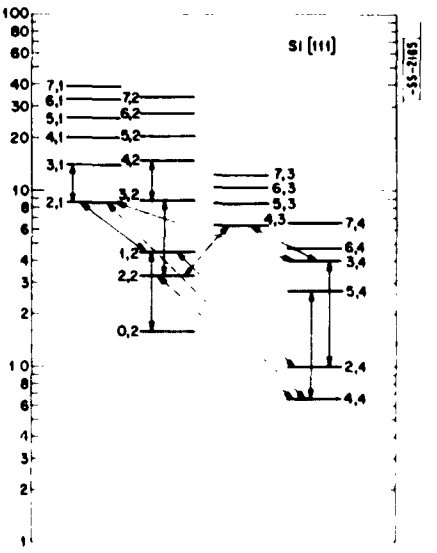

Fig. V-6. Low-lying energy levels of holes in the valence bands of Si. The full lines show prominent transitions observed in the spectra. The dotted lines show $\Delta n = \pm 2$, $\Delta n = \pm 3$ transitions observed.

B. PARAMAGNETIC RESONANCE

Several natural crystals have been investigated by electron spin resonance techniques at 1 cm and 4 mm to determine (1) the paramagnetic impurities present and (2) the applicability to millimeter-wave maser systems by virtue of the zero-field splittings and relaxation times observed. Of the crystals investigated, kyanite (Al_2SiO_5) showed zero-field splittings at 20, 60 and 80 kMcps and these splittings are attributed to Fe^{3+} impurities. The CW saturation relaxation times at 4.2°K of two lines at 20 kMcps were about 10^{-3} second. This material therefore meets the preliminary requirements of a millimeter-wave maser material. However, there was at least one other impurity observed but not identified. This material should be synthesized and studied in greater detail for millimeter-wave maser application.

W. H. From

C. MICROWAVE PHONON GENERATION BY SPIN WAVE RESONANCE

Experiments in which microwave phonons are generated by spin wave resonance (SWR) in thin Permalloy films are continuing. An improved detection system at 9 kMcps has been developed which permits simultaneous observation of piezoelectric-generated and SWR-generated phonon echoes in the same rectangular cavity.

The relationship between SWR order number (k-value) and phonon echo amplitude is being studied in films of various thicknesses and compositions which have been evaporated onto both AC- and X-cut quartz crystals. Qualitatively it is found that in the thinner films, which exhibit only a few SWR peaks, the maximum phonon echo amplitude occurs on the main peak, but in the thicker films the maximum occurs on one of the SWR peaks. This is an indication of approach to the cross-over condition (equality of phonon and magnon wavelength) since in the thinner films the main resonance peak is really a spin wave peak under spin-pinning conditions.* The main peak in the thicker films involves lower k-values (not satisfying the SWR condition) which are further from crossover.

Echoes have also been generated in the parallel case on ferromagnetic resonance in films deposited on AC- and X-cut quartz crystals. A large uniaxial magnetic anisotropy was found in the film plane. In the easy direction one of the two transverse phonon modes is generated, whereas in the hard direction the other mode is generated. This indicates a possible relationship between the magnetic anisotropy axis and quartz crystal axes.

M. H. Seavey, Jr.

D. SUPERCONDUCTING MAGNETS

1. Niobium-Zirconium Alloys

A large number of additional samples of Nb-Zr alloy wire have been examined in the M. I. T. Bitter magnet at fields up to 88 kgauss. These samples had various compositions and heat treatments. In all cases the current-carrying capacity of the short samples tested fell off sharply at about 70 kgauss, which thus appears to be an upper limit for superconducting magnets of this material. The current-carrying capacity at lower fields was better for some heat treatments than for others. However, as mentioned in the last quarterly progress report, the low-field

*M.H. Seavey, Jr., "Electromagnetic Theory of Spin Wave Resonance," Technical Report No.239 [U], Lincoln Laboratory, M.I.T. (15 February 1961), ASTIA 255342.

behavior of coils of Nb-Zr wire cannot be accurately predicted on the basis of measurements on short samples. Therefore, it will not be possible to determine whether the low-field current-carrying capacity of coils can be enhanced by using this heat treatment until long lengths are available for tests.

A number of solenoids have been made with Nb-Zr wire; the highest field generated so far is 56 kgauss. There are, however, a number of problems concerned with the reliability which remain to be solved. When nylon or formvar insulation is used, high voltages can appear across parts of the coil if it becomes resistive. This may cause arcing and breakdown of the insulation as well as local annealing of the wire. Methods of avoiding these troubles are being investigated.

It has been found that flexing of the wire can result in temporary loss of superconductivity. This was established by moving a loop of wire which was immersed in liquid helium by means of a string attached to it. Even in the absence of a magnetic field, a 10-mil Nb-Zr wire momentarily became normal when quickly bent through a distance of about 1 mm. An approximate calculation of the heat generated in the wire during this motion indicates that a temperature rise should result which is more than adequate to raise the superconductor above its transition temperature. This indicates that, in the design of magnets using this material, it is important that all wire, including the leads, be constrained against motion.

2. Sintered Niobium-Tin

A number of experiments have been carried out on cylinders made of mixtures of Nb and Sn powders which were hydraulically pressed and then heat-treated. These results are described in some detail in an article to be published in the Proceedings of the International Conference on High Magnetic Fields. The results obtained so far may be briefly summarized as follows.

Fields up to 25 kgauss have been trapped in $\frac{1}{2}$-inch o.d. cylinders with $\frac{1}{4}$-inch-diameter holes drilled along the axis. This was done by exposing the cylinders (T = 4.2°K) to the field of a Bitter magnet. The hole in the cylinder was shielded from the external field up to a critical point, whereupon the field suddenly broke through. The field inside the hole remained constant when the external field was lowered to zero and continued to be maintained by persistent currents as long as the cylinders were kept cold. The current density in the cylinder walls is calculated to be at least 10^5 amp/cm^2, which is comparable with the values reported for Nb Sn-core wire.*

The work on sintered Nb-Sn has been carried out in collaboration with F. Rothwarf of the Frankford Arsenal. K. Gooen of the National Magnet Laboratory and Lucien Donadieu of RLE have participated in much of the other work.

S. H. Autler

E. PHONON STUDIES IN SUPERCONDUCTORS

A number of properties of materials in the superconducting state are being studied by means of phonon interactions. Initially, pulsed ultrasonic attenuation measurements at 30 Mcps were carried out in niobium as a function of temperature, from room temperature to 4.2°K. As expected, the attenuation decreased rapidly with decreasing temperature, particularly through the superconducting transition. At low temperatures a number of oscillations were observed in the amplitude of attenuation as a function of temperature.† The ratio of ultrasonic attenuation in the

---

* J.E. Kunzler, et al., Phys. Rev. Letters 6, 89 (1961).

† The same phenomenon has been reported in Va and Ta by Levy and Rudnick, Bull. Am. Phys. Soc. 6, 501 (1961).

normal-to-superconducting state will yield the temperature-dependent superconducting energy gap. In addition, application of a magnetic field is expected to result in band structure information.

R. Weber

F. RESONANCE IN SPIRAL SPIN CONFIGURATIONS

It should be possible to observe magnetic resonance for spiral spin configurations excited by uniform RF magnetic fields. As a simple example, consider the case of a line of identical spins with an easy plane at right angles to the direction of the line.* At equilibrium, the spins will lie in the easy plane, with an angle Θ between nearest-neighbor pairs of spins projected on a common plane perpendicular to the spin line (Fig. V-7). Suppose we assume nearest-neighbor exchange of the form $-J_1\vec{S}_n \cdot \vec{S}_{n+1}$ (ferromagnetic) and second nearest-neighbor exchange $+J_2\vec{S}_n \cdot \vec{S}_{n+2}$ (antiferromagnetic). The equation of motion of the n^{th} spin is then

$$\frac{d\vec{S}_n}{dt} = \gamma\vec{S}_n \times \left| J_1(\vec{S}_{n+1} + \vec{S}_{n-1}) - J_2(\vec{S}_{n+2} + \vec{S}_{n-2}) \right| + \vec{T}_n \quad , \tag{1}$$

where $\vec{T}_n$ is the anisotropy torque acting on the spin $\vec{S}_n$.

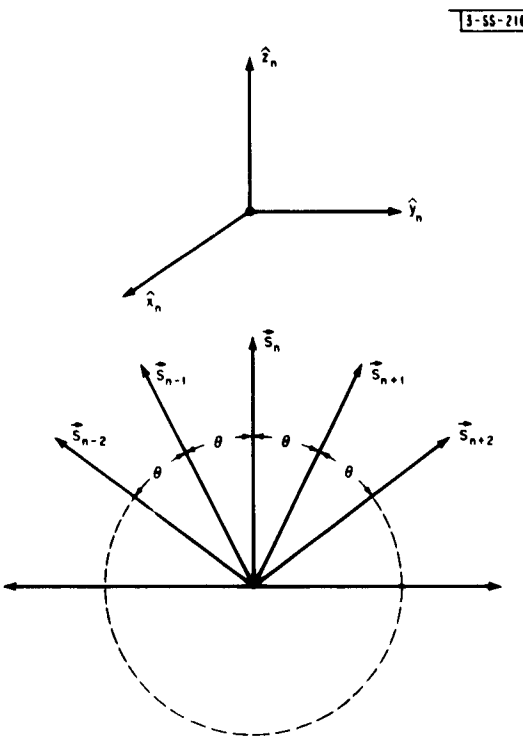

Fig. V-7. Schematic representation of a spiral spin configuration for the case of an easy anisotropy plane.

At equilibrium the torque acting on $\vec{S}_n$ will be zero. This is not a sufficient condition, however, to determine the equilibrium configuration in the easy plane since for any angle Θ, the bracketed term in (1) is a vector parallel to $\vec{S}_n$; and since $\vec{T}_n = 0$ in the plane, $d\vec{S}_n/dt = 0$ automatically. To determine Θ, the energy of the n^{th} spin is written

* The present calculation is an extension of the works of A. Yoshimori [J. Phys. Soc. Japan 14, 807 (1959)], T. Kaplan [Phys. Rev. 116, 888 (1959)] and J. Villain [J. Phys. Chem. Solids 11, 303 (1959)].

$$E = -\vec{S}_n \cdot [J_1(\vec{S}_{n+1} + \vec{S}_{n-1}) - J_2(\vec{S}_{n+2} + \vec{S}_{n-2})]$$

$$= 2S^2[-J_1 \cos\Theta + J_2 \cos 2\Theta] \quad .$$

Requiring $\partial E/\partial\Theta = 0$ at equilibrium gives

$$\sin\Theta[+J_1 - 4J_2 \cos\Theta] = 0$$

or

$$\sin\Theta = 0 \quad , \quad \cos\Theta = \frac{J_1}{4J_2} \quad .$$

It can be easily verified that $\cos\Theta = J_1/4J_2$ gives the lowest energy for $J_1/4J_2 < 1$. We shall call the equilibrium value of $\vec{S}_n$, $\vec{S}_n^o$.

Suppose now that oscillations about equilibrium occur such that

$$\vec{S}_n = \vec{S}_n^o + \vec{s}_n \exp[i(kn + \omega t)] \quad .$$

The vector $\vec{s}_n$ is a constant vector, and $\vec{s}_{n+1}$ is the same with respect to $(\hat{x}_{n+1}, \hat{y}_{n+1}, \hat{z}_{n+1})$ as $\vec{s}_n$ with respect to $(\hat{x}_n, \hat{y}_n, \hat{z}_n)$. We assume that the anisotropy energy of a spin is of the form $E_A = -\frac{1}{2}\gamma H_A S \sin^2\psi$, where ψ is the angle of tipping of a spin out of the easy plane. The torque acting on $\vec{S}_n$ for displacement $d\psi$ is

$$\vec{t}_n = \frac{-\partial E_A}{\partial\psi}\,\hat{y}_n = -\gamma H_A S \sin\psi \cos\psi \hat{y}_n$$

$$\cong -\gamma H_A S\, d\psi\, \hat{y}_n = -\gamma H_A s_{nx}\, \hat{y}_n \quad .$$

Then in the coordinate system $(x_n, \hat{y}_n, \hat{y}_n)$ the linearized equations of motion of $\vec{s}_n$ lead, after simplification, to

$$i\omega s_{nx} = \gamma s_{ny}[2J_1 S \cos\Theta(1 - \cos k) - 2J_2 S \cos 2\Theta(1 - \cos 2k)]$$

$$i\omega s_{ny} = -\gamma s_{nx}[2J_1 S(\cos\Theta - \cos k) - 2J_2 S(\cos 2\Theta - \cos 2k) + H_A] \quad . \qquad (2)$$

The resonance frequency is given by setting the determinant of Eq. (2) equal to zero.

Let us now consider a set of $2N + 1$ spins, with $n = -N, -N + 1, 0, N - 1, N$. The net magnetization in the direction of an axis fixed in space parallel to $\hat{y}_o$ is

$$m_y = \sum_{m=-N}^{+N} m_{oy}\, e^{i(kn+\omega t)} \cos n\Theta$$

$$= m_{oy}\, e^{i\omega t}\left(1 + \sum_{n=1}^{N} 2 \cos nk \cos n\Theta\right) \quad .$$

This sum will be very small for large N, unless $k = \Theta$. For this case

$$m_y \simeq m_{oy}\, e^{i\omega t}(N + 1) \quad .$$

There is thus a net moment which can be driven by a uniform external RF magnetic field at a frequency ω given by

$$\omega = \gamma\{[2J_1 S \cos\Theta(1 - \cos\Theta) - 2J_2 S \cos 2\Theta(1 - \cos 2\Theta)]\,[H_A]\}^{1/2} \quad .$$

We plan to search for such resonances at millimeter wavelengths in a number of materials that have spiral spin configurations.

H. J. Zeiger

COMPUTER COMPONENTS

GROUP 53

J. B. Goodenough, *Leader*

D. O. Smith, *Associate Leader*

Arnott, R. J.
Baker, A. G.
Barck, P. E.
Burke, R. L.
Cohen, M. S.
Delaney, E. J.
Dwight, K., Jr.
Eckl, D. J.
Ferretti, A.
Fitzgerald, J. F.
Harte, K.*
Huber, E. E., Jr.†
Johnston, R. C.
Kaplan, T. A.
Kirk, C. T.
Kunnmann, W.
Larson, E. G.*
Lehrer, S. S.
Menyuk, N.
Moon, R. M., Jr.†
O'Keefe, J. J.
Ridgley, D. H.
Rogers, D. B.†
Weiss, G. P.
Whipple, E. R.
Wold, A.

---

* Part Time
† Staff Associate

TABLE VI-1
PROPERTIES OF THE SYSTEM $CoV_{2-x}Al_xO_4$

Sample	Cell Edges (Å)		V-V (Å)	Activation Energies (ev)	
	Measured	Vegard		High T	Low T
CoV_2O_4	8.407 ± .002		2.97	0.08	0.06
$CoV_{1.5}Al_{0.5}O_4$	8.332 ± .002	8.332	2.95	0.12	0.10
$CoV_{1.2}Al_{0.8}O_4$	8.286 ± .002	8.286	2.93	0.18	0.10
$CoV_{0.8}Al_{1.2}O_4$	8.233 ± .002	8.228	2.91	0.34	
$CoAl_2O_4$	8.103 ± .002				

TABLE VI-2
PREPARATION AND PROPERTIES OF THE SYSTEM $Fe_{1+x}V_{2-x}O_4$

Sample	Ratio $CO:CO_2$	Theoretical Oxidation State (per cent)	a_o (Å)	q (ev)	θ ($\frac{\mu v}{deg}$)
FeV_2O_4	~9:2	100 ± 0.1	8.454	0.248	+414
$Fe_{1.05}V_{1.95}O_4$	~9:2	99.5 ± 0.3	8.455	0.278	+378
$Fe_{1.1}V_{1.9}O_4$	~8.5:2.3	100.1 ± 0.1	8.455	0.337	+364
$Fe_{1.15}V_{1.85}O_4$	~8.5:2.3	100.1 ± 0.1	8.455		
$Fe_{1.2}V_{1.8}O_4$	~8:2.5		8.454		
$Fe_{1.25}V_{1.75}O_4$	~8.5:3.0	99.2 ± 0.1	8.452	0.236	
$Fe_{1.5}V_{1.5}O_4$	~2:1	100.8 ± 0.2	8.449	0.17	
$Fe_{1.625}V_{1.375}O_4$	~4:3		8.443		
$Fe_{1.75}V_{1.25}O_4$	~1:1		8.433		
Fe_2VO_4	~1:3	99.9 ± 0.1	8.417	0.31	−47

VI. TRANSITION-METAL COMPOUNDS

A. SPINELS

1. Transport Properties of Some Vanadites

Results of our continued research during the past quarterly period on the preparations and property characterizations of spinels containing V^{+3} and V^{+4} are summarized below.

a. The System $CoV_{2-x}Al_xO_4$

A repeat of our work on the system $CoV_{2-x}Al_xO_4$, utilizing nonhygroscopic aluminum oxide as a starting material, is nearing completion. Cell edges, V-V distances and measured activation energies are reported in the accompanying Table VI-1. Differences in activation energies at low temperatures and in the cell edges for the intermediate members of the series from tne data previously reported can now be attributed to oxidation in our original samples. Cell edges of the new series obey Vegard's law very well, and all activation energies apparently increase in a uniform manner with increasing Al content. Transitions occurring at low temperatures in the activation energies of these materials are probably due to magnetic ordering. In the case of $CoV_{1.2}Al_{0.8}O_4$, with more than 50 per cent of the B-sites occupied by V^{+3}, the V-V distance has been reduced to 2.93Å, and yet there appears to be no semiconductor $\Longleftrightarrow$ metallic transition over the temperature interval measured.

b. The System $Fe_{1+x}V_{2-x}O_4$

Good progress has been made on the preparation of intermediates in the system $Fe^{+2}_{1.0}[Fe^{+2}_xV^{+3}_{2-2x}V^{+4}_x]O_4$. Table VI-2 summarizes preparation procedures and physical properties. All activation energies (q) reported are those for high temperature (above T_c).

c. CdV_2O_4

In order to check the effect of large V-V separations on the measured activation energies in vanadium spinels, a sample of CdV_2O_4 was prepared. The cell edge is 8.689Å and the activation energy 0.27 ev. It is noteworthy that the activation energy for CdV_2O_4 does not differ greatly from either that of FeV_2O_4 (0.25 ev) or that of MnV_2O_4 (0.28 ev).

D. B. Rogers
R. J. Arnott
E. J. Delaney

2. Magnetic Transitions in Some Chromites and Vanadites

A study has been made of the magnetic properties of the cubic spinels $MnCr_2O_4$, $CoCr_2O_4$, MnV_2O_4 and CoV_2O_4 from the Curie point to 4.2°K. Stoichiometric chromite samples were prepared by the precursor method as described in detail by Whipple and Wold.[1] The vanadites were prepared by first grinding mixtures of CoO and V_2O_3 or MnO and V_2O_3 in a nitrogen dry box. The cobalt-vanadium oxide mixture was then heated to 1100°C in an evacuated sealed silica capsule, and the manganese-vanadium oxide mixture was heated to 1100°C in hydrogen atmosphere. Chemical analysis of the resulting samples indicated that the ratio of B-site to A-site cations was within 0.3 per cent of 2:1.

The magnetization curves of these materials, as obtained on the vibrating-coil magnetometer in a field of 11,000 oe, are shown in Fig. VI-1. With the possible exception of MnV_2O_4, all the

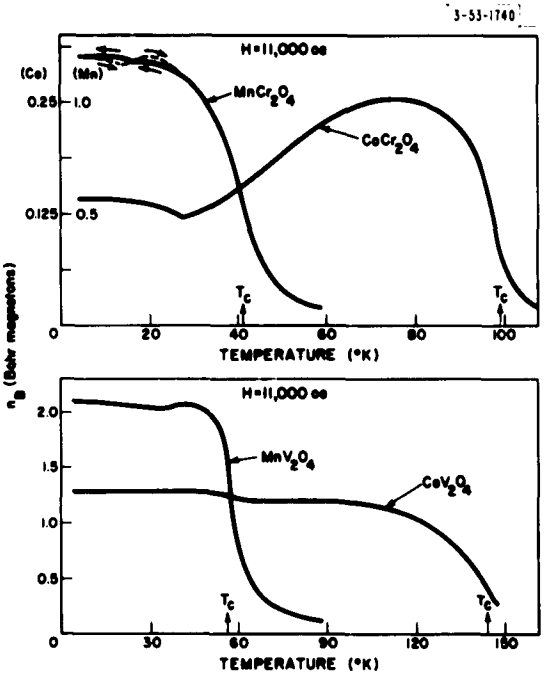

Fig. VI-1. Magnetization curves taken in a field of 11,000 oe. The Curie points shown are based on determinations made with low-field values (H ≅ 100 oe).

curves evidence a magnetic transition between the Curie point and 4.2°K. These materials have all been reported to be normal spinels.[2,3,4] Thus these magnetic properties should be interpretable in terms of the recent theory of spin configurations in the ground state (T = 0) and at the Curie point ($T = T_c$).[5,6] However, contradictions between our low-temperature data and predictions based on the ground-state theory led us to question the statement that these are all normal spinels. The CoV_2O_4 sample was therefore heated to 1100°K and slowly cooled in an evacuated tube. This treatment led to significant changes in the magnetic properties of CoV_2O_4, which appears to confirm the fact that this material is not, in general, a normal spinel.

On the other hand, the chromites are presumably normal, since a similar retreatment of $CoCr_2O_4$ produced no significant change in its magnetic properties, and the normality of $MnCr_2O_4$ has been determined accurately by Corliss and Hastings.[7] This is in agreement with theoretical calculations that indicate Cr^{3+} ions have a strong preference for octahedral sites. The sharp transitions observed in the magnetization curves of the chromites should be interpreted on the basis of the spin-configuration theory in normal spinels. This interpretation requires that the observed transition in $MnCr_2O_4$ be due to a change from a collinear (Néel-type) spin configuration to the ferrimagnetic spiral which has been explicitly defined,[5,6] whereas the transition in $CoCr_2O_4$ is due to a shift from the defined spiral to a more complicated spin configuration. The interpretation for $MnCr_2O_4$ is compatible with the experimental neutron diffraction work of Corliss and Hastings.[7] Furthermore, the interpretation for $CoCr_2O_4$ is consistent with a molecular field calculation of the magnetization curve predicted for a collinear configuration, since a large deviation from the experimentally observed curve occurs at temperatures far above the transition temperature.

N. Menyuk D. B. Rogers
A. Wold K. Dwight, Jr.

3. Jahn-Teller vs Spin-Orbit Coupling Transitions

The low-temperature crystallographic distortions from cubic symmetry found in FeO and CoO carry a sign characteristic of spin-orbit coupling and a collinear spin configuration for $T < T_N$. This sign is opposite that which would optimize Jahn-Teller stabilizations. In $Cu[Cr_2]O_4$ and $Ni[Cr_2]O_4$, on the other hand, they carry the sign of the Jahn-Teller effect, which tends to quench spin-orbit coupling, even though the orbital angular momentum associated with tetrahedral-site Cu^{2+} and Ni^{2+} is no more quenched than for octahedral-site Fe^{2+} and Co^{2+}. This leads to the conclusion that, for a free-ion complex, distortions of either sign give nearly the same stabilization, so that the sign observed in any particular situation depends upon long-range coupling. If $2\delta_t$ is the magnitude of a Jahn-Teller stabilization, then $\lambda \mathbf{L} \cdot \mathbf{S} + \delta_t$ is the spin-orbit stabilization for the free-ion complex. Therefore, if

$$\lambda \mathbf{L} \cdot \mathbf{S} > \delta_t \quad , \quad \text{spin-orbit effects dominate;}$$

$$< \delta_t \quad , \quad \text{Jahn-Teller effects dominate.}$$

For a solid, δ_t varies as the fraction of lattice sites that are occupied by the Jahn-Teller ion; and $\lambda \mathbf{L} \cdot \mathbf{S}$ is a maximum below a magnetic ordering temperature that aligns all spins $\mathbf{S}_i$ collinear. In $Ni[Cr_2]O_4$ and $Cu[Cr_2]O_4$ the Néel, collinear spin configuration does not occur, and Jahn-Teller effects predominate. However, at T = 4°K the nominal compound $Ni^{2+}_{0.5}Fe^{3+}_{0.5}[Ni^{2+}_{0.5}Cr^{3+}_{1.5}]O_4$ has collinear A-site spins,[8] which optimizes $\lambda \mathbf{L} \cdot \mathbf{S}$. In this case the distortion should carry the sign of the spin-orbit coupling, since δ_t per Ni^{2+} is simultaneously reduced; and the sign of the distortions observed in the system $NiCr_tFe_{2-t}O_4$ should change in the interval $1.5 < t < 2.0$. Such a change has been observed at $t \approx 1.8$ (Ref. 9).

J. B. Goodenough

4. Growth of Cobalt-Ferrite Single Crystals

Two methods are separately being applied toward the growth of cobalt-ferrite single crystals: growth by slow-cooling a melt under a temperature gradient at high oxygen pressures and growth from a flux under normal air pressure.

a. Crystal Growth from the Melt

Above the melting point of $CoFe_2O_4$, the rate of increase of the equilibrium oxygen pressure with temperature increases sharply. In order to decrease the Fe^{+2} content, one could go to much higher pressures with the possibility of a higher melting temperature, or introduce impurities into the melt to lower its melting point. It is desirable to operate below 1600°C in the molten state, since above this temperature the necessary equilibrium pressure becomes quite high. There are a number of ways of introducing a removable impurity into the material; two of these are:

(1) Let the ferrite decompose slightly, thereby lowering its melting point. With increased oxygen pressure, it might be possible to remove the Fe^{+2} in the molten state, thereby causing the melt to solidify as the stoichiometry is corrected.

(2) Use a foreign impurity that would separate completely upon freezing of the melt.

A number of runs were made to test the first part of method 1. At 900 psig O_2 pressure and 1620°C, some melting occurred. The resulting material had the appearance of a two-component

system, consisting of a melted matrix containing unmelted particles. This would account for the difficulty encountered in determining the melting points at low pressures. At 475 psig O_2 and 1625°C, a clean, fluid melt occurred. At 475 psig O_2 and 1600°C, a two-component melt reoccurred.

Since clean melts did not occur at 1600°C and below, it was decided to attempt method 2. A mixture of 5 per cent $Na_2Fe_2O_4$ in $CoFe_2O_4$ was fired in a range of 1560° to 1600°C at an O_2 pressure of 1400 psig. A clean melt resulted, and subsequent analysis showed the Fe^{+2} content to be 0.1 ± 0.1 per cent.

b. Crystal Growth from a Flux

The so-called "cold-finger" technique of crystal growth is being used. During the last quarter a successful attempt was made which yielded four 1-inch conical-shaped crystals. Because of possible thermal shock or other factors, the four crystals did not remain intact, but broke up into several large sections (large enough for use). Since the primary interest of the physicists lies with $NiFe_2O_4$ and $NiFe_2O_4$ with $CoFe_2O_4$ additions, the technique is now being applied to these materials; the assumption is that the phase data for $NiFe_2O_4$ and $CoFe_2O_4$ should be relatively similar.

W. Kunnmann
A. Ferretti
A. Wold

B. NICKEL ARSENIDES

1. Magnetic Properties of Cr_5S_6 in Chromium Sulfides

We have prepared several samples of chromium sulfide CrS_x with x between 1.145 (Cr_7S_8) and 1.200 (Cr_5S_6). Spectroscopically pure powdered chromium and compressed pellets of sublimed sulfur were weighed, mixed and sealed in evacuated silica tubes. Some samples (slow-cooled) were then heated at 17°/hour to 400°C, held there for 24 hours, heated to 1000° at 25°/hour, held there for 24 hours, and then cooled slowly at 30°/hour. After being reground and pressed into bars, these samples were reheated to 1000°C at 50°/hour, held there for 30 hours, and again cooled at 30°/hour. Other samples (quenched) were heated at 50°/hour to 1000°C, held there for three days, and then quenched in ice water. After being reground and resealed, they were again heated to 1000°C at 50°/hour, held there for a week, and quenched in ice water. After preparation, the final samples were carefully analyzed for total chromium[10] and the sulfur content was determined from the weight difference, so that our values for x represent the actual compositions of the final samples.

Cr_7S_8 has the nickel-arsenide structure, with cation vacancies ordered into alternate layers, but disordered within each layer. Cr_5S_6 also is based on the nickel-arsenide structure, but with a complete ordering of the cation vacancies which give rise to superlattice lines in the x-ray diffraction pattern. Jellinek[11] has indicated that the intermediate compositions consist of mixtures of these two phases. X-ray analysis of our samples showed only the presence of these two phases; i.e., nickel-arsenide plus superlattice lines. The Cr_5S_6 superlattice lines were distinct in samples A (slow-cooled with x = 1.194) and B (quenched with x = 1.178), were barely discernible in sample C (slow-cooled with x = 1.155), and were not detectable in sample D (quenched with x = 1.155).

The magnetic properties of these samples were determined with a vibrating-coil magnetometer, and the results for samples A and B are shown in Fig. VI-2. These samples possess

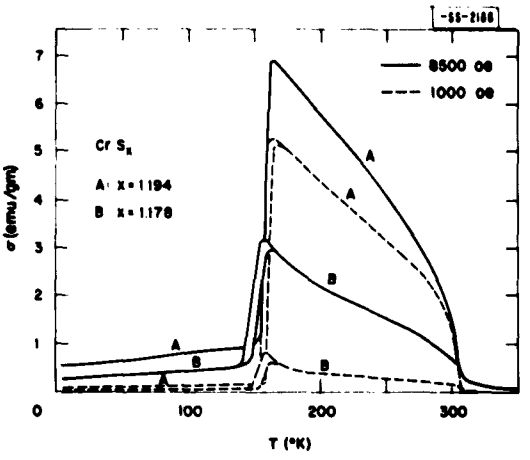

Fig. VI-2. The temperature variation of the magnetization of samples of CrS_x with x = 1.194 (A) and x = 1.178 (B) in external fields of 1000 and 8500 oe.

a striking ferrimagnetic-antiferromagnetic transition in the neighborhood of 155°K. The ferrimagnetic nature of the spontaneous magnetization was demonstrated by the high-temperature susceptibility measurements of Yuzuri, et al.,[12] whereas the antiferromagnetic nature of the low-temperature state is shown by the decrease in susceptibility with decreasing temperature indicated in Fig. VI-2. Our experimental values for the Curie temperature T_c, the maximum magnetization in an applied field of 8500 oe σ_{max}(8500 oe), the cooling transition temperature in a field of 1000 oe T_{tc}(1000 oe), the width of the transition δ_t, the thermal hysteresis $T_{tw} - T_{tc}$, and the shift in the transition temperatures caused by increasing the applied field from 100 to 8500 oe Δ_H are summarized in Table VI-3, together with the results of 4-terminal AC resistivity measurements.

Since the Curie point is independent of composition, a single magnetic phase must be responsible for the ferrimagnetism, and hence for the transition, in all these materials. Since sample A (which is almost pure Cr_5S_6) possesses both the largest magnetization and the sharpest transition, we conclude that it is the Cr_5S_6 phase alone which is responsible for the observed properties.

The ordered structure[11] of Cr_5S_6 suggests a plausible model for its magnetic behavior. In NiAs structures, the dominant exchange interaction is an antiferromagnetic one along the c-axis. In Cr_5S_6, every fourth member of a chain is missing, so that each chain possesses a net moment. There are two distinguishable sets of chains, and the material as a whole is ferrimagnetic or antiferromagnetic, depending upon whether the interchain coupling is ferromagnetic or antiferromagnetic. There are two competing contributions to this interchain coupling: a ferromagnetic, 90° cation-anion-cation interaction and an antiferromagnetic cation- -cation interaction.

If we assume a delicate balance between the two types of coupling (as indicated by our large value for Δ_H), we see that the high sensitivity of the antiferromagnetic cation- -cation coupling to lattice spacing could easily cause the observed ferrimagnetic-antiferromagnetic transition.[13] This same sensitivity to lattice spacing can be expected to give rise (e.g., through volume magnetostriction) to a first-order transition possessing thermal hysteresis. Finally, the above model is consistent with the decrease of T_t with decreasing x. Decreasing x increases the lattice spacing,[11] and thereby increases the amount of thermal contraction required to obtain the transition.

TABLE VI-3
THE DEPENDENCE OF CERTAIN PROPERTIES OF CrS_x UPON COMPOSITION

Sample	A	B	C
x	1.194	1.178	1.155
T_c	305°K	305°K	*
σ_{max} (8500 oe)	6.9 emu/gm	3.0 emu/gm	0.3 emu/gm
δ_t	5°K	8°K	15°K
T_{tc} (1000 oe)	158°K	151°K	68°K
$T_{tw} - T_{tc}$	4°K	6°K	–
Δ_H	4°K	4°K	–
ρ (300°K)	1.06×10^{-3} ohm-cm	1.00×10^{-3} ohm-cm	0.94×10^{-3} ohm-cm
ρ (77°K)	0.50×10^{-3} ohm-cm	0.40×10^{-3} ohm-cm	0.58×10^{-3} ohm-cm

* Signal too small for accurate determination.

It should be pointed out that all our samples had metal-like conductivities that evidenced no anomaly at the magnetic transition and that were virtually independent of composition. Thus it appears that the conductivity mechanism is not affected by any magnetic ordering and that it is not intimately connected either with the presence or ordering of cation vacancies.

K. Dwight, Jr. N. Menyuk
R. W. Germann A. Wold

2. Cation- -Cation Bonding in FeS

It is pointed out[14] that the peculiar behavior of the magnetic susceptibilities through the spin-flip temperature T_s and the crystallographic transition T_α as well as the low-temperature structure can be accounted for if the critical separation between Fe^{2+} ions in a sulfur matrix is $R_c \approx 3.0$ Å. For $R < R_c$ the overlapping d orbitals form collective, molecular orbitals; for $R > R_c$ the outer d electrons are localized. Although crystalline fields stabilize a Γ_{T1} configuration, cation- -cation interactions between c-axis pairs stabilize a degenerate $\Gamma_{T3}^{1,2}$. This latter interaction is stronger at lower temperatures where the c parameter is smaller. For $T_s < T < T_N$, dipole-dipole interactions keep the spins in the basal plane, but below T_s spin-orbit coupling predominates to make an easy c-axis and further stabilize $\Gamma_{T3}^{1,2}$. Below T_α, three-membered rings of Fe^{2+} ions are formed. The molecular orbitals of these rings are more than half-filled, so that the basal planes remain ferromagnetic. Presumably elastic energies are responsible for three-membered ring formation rather than the more stable homopolar-bond formation.

J. B. Goodenough

3. Single-Crystal MnP

MnP has the B31 structure, which is distorted NiAs. Goodenough[13] has attributed the distortions to cation- -cation d bonding. Chemical and spectroscopic analyses have been carried out on portions of a manganese-phosphide single crystal prepared previously. The chemical analysis showed 100.0 per cent of theoretical manganese for MnP; the precision of the analytical method is in the range of 0.3 per cent.

Spectrographic analysis showed only the impurities Mg (0.001 to 0.01 per cent), Si (0.001 per cent), Fe (<0.0001 per c nt) and Pb (0.001 per cent). Numerous other elements were sought but were not detected in the nalysis.

D. H. Ridgley
E. R. Whipple

C. SUBSTITUTED TUNGSTEN BRONZES

The system may be formulated in a general manner as $Na_{(x+y)}W^{VI}_{1-(x+y)}W^{V}_{x}Ta^{V}_{y}O_3$. This represents a series with part of the nominal tungsten (V) of the well-known "tungsten bronze" series (the case with y = 0) replaced by tantalum (V).

Attention for the present is being focused upon the case where x = 0, i.e., all metal ions in the highest valence state with essentially no free or conduction electrons. Representatives over the complete range of values of y (x = 0) have been prepared and attempts are being made to characterize the products. Diffraction lines related to cubic symmetry have been found to dominate the x-ray patterns of products with x = 0, y = 0.90, 0.80 and 0.65 (nominal). No success has been achieved in preliminary attempts to assign a few additional weak lines in each of these patterns. With x = 0, y = 0.10 (nominal), the x-ray pattern compares very closely with that reported for WO_3.

A number of annealing, quenching and slow-cooling experiments have been made on some of the above products with apparent inconsistencies in results. All the above materials were prepared in air and varied in color from white for the high sodium-tantalum compositions to light yellow for those with low sodium-tantalum contents. Firing the materials in sealed, quartz ampoules to obviate a possible volatilization of a component that might occur during air-firing has yielded only medium-blue products.

D. H. Ridgley
E. J. Delaney

REFERENCES

1. E.R. Whipple and A. Wold, J. Inorg. and Nucl. Chem. (to be published).
2. E.J.W. Verwey and E.L. Heilmann, J. Chem. Phys. 15, 174 (1947).
3. A. Burchese, Ann. Chim. (Rome) 47, 827 (1957).
4. H.M. Richardson, F. Bell and G.R. Rigby, Trans. Brit. Ceram. Soc. 53, 376 (1954).
5. D. Lyons, T.A. Kaplan, K. Dwight and N. Menyuk, J. Appl. Phys. 32S, 13 (1961).
6. D. Lyons, T.A. Kaplan, K. Dwight and N. Menyuk, Phys. Rev. (to be published).
7. L. Corliss and J. Hastings, J. Appl. Phys. (to be published).
8. S.J. Pickart and R. Nathans, Phys. Rev. 116, 317 (1959).
9. T.R. McGuire and S.W. Greenwald, Solid State Physics in Electronics and Telecommunications, Vol. 3, Part I, "Magnetic and Optical Properties," Eds. M. Desirant and J.L. Michiels (Academic Press, London, 1960), p. 50.
10. We are indebted to E.R. Whipple for some of these analyses.
11. F. Jellinek, Acta Cryst. 10, 620 (1957).
12. M. Yuzuri, T. Hirone, H. Watanabe, S. Nagasaki and S. Maeda, J. Phys. Soc. Japan 12, 385 (1957).
13. J.B. Goodenough, Magnetism and the Chemical Bond (Interscience Publishers, Inc., New York), supp. to Progress in Inorganic Chemistry, Ed., F.A. Cotton (to be published).
14. J.B. Goodenough, J. Appl. Phys. (to be published).

VII. MAGNETIC FILMS

A. ANOMALOUS MAGNETIC FILMS

1. Introduction

Thus far three kinds of anomalous magnetic films have been reported: mottled, rotatable-anisotropy and inverted films. Huber and Smith[1] found that the high-field hysteresis loops of mottled films are the same when measured in any azimuth: they show low remanence and a high coercive force. Bitter patterns of mottled films present a spotted or mottled appearance. These mottled films have the property that the value of the initial susceptibility (and thus the apparent position of the easy axis) as found from low-field hysteresigraph behavior is determined by previously applied high magnetic fields.[2] Prosen[3] has applied the name "rotatable anisotropy" to this property which he found in films made by a special technique; other investigators have also studied the effect.[4,5,6] Still another kind of anomalous film is the inverted film,[7] which has the property that the wall coercive force H_w is greater than the rotational coercive force H_k.

In the present investigation, Permalloy films with these anomalous properties have been made by several methods which differ from those reported previously. The experimental study of these films points to a connection between the various types of anomalous films. A model is presented to explain the experimental results.

2. Rotatable Initial-Susceptibility Films

A simple, but unambiguous test for anomalous films can be made with the aid of a hysteresigraph.[8] This instrument has shown that, for many of the films examined in the present investigation, the value of the initial susceptibility is determined by previously applied high fields as described above, but the high-field hysteresis loops are nearly square and remain almost the same when measured in any azimuth [Fig. VII-1(i-ii)]. The value of the remanent magnetization is thus almost equal to the saturation magnetization for these films, although occasional films have shown a remanence as low as 90 per cent of the saturation magnetization. The Bitter patterns of such films show little mottling. In this report they will be called rotatable initial-susceptibility (RIS) films to distinguish them from low-remanence films: (a) mottled films, for which the initial susceptibility can also be "rotated" but which have low remanence [Fig. VII-1(iii)] and mottled Bitter patterns, and (b) Prosen's rotatable-anisotropy films, whose high-field loops are similar to those of mottled films.

In the present study two different types of RIS films can be distinguished: For the first type the initial susceptibility, as measured by a low drive field, is zero in the arbitrary direction in which a high AC field has been previously applied, but attains a maximum 90° away. For a type 2 film, on the other hand, the initial susceptibility is maximum parallel to the high AC field direction, but zero 90° away. Nevertheless, if a high DC field is applied in an arbitrary direction to either type of film, the initial susceptibility behavior is like that of a type 1 film after subjection to a high AC field. For some films the application of a high AC field in an arbitrary direction will establish neither a maximum nor a zero initial susceptibility in that direction, but will merely change the magnitude of the initial susceptibility. In this case the RIS effect is not strong enough to overcome the original field-induced anisotropy completely, and the films are said to tend toward type 1 or 2 RIS.

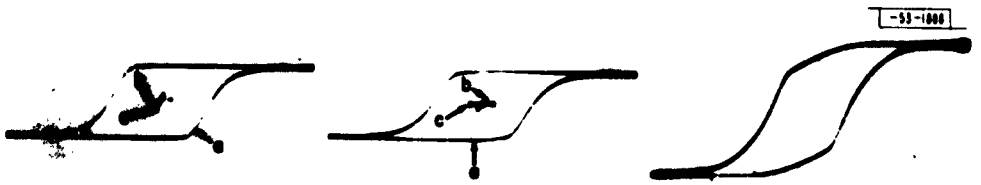

Fig. VII-1. (i) Hysteresis loop of a type 1 RIS film with composition 85 per cent Ni, 15 per cent Fe, thickness 900 Å, made at an evaporation rate of 130 Å/minute at a substrate temperature of 300°C (a is the major loop when peak drive field was 70 oe, b is the low-drive response in a direction parallel to that of a previous high drive, c is the low-drive response in a direction perpendicular to that of a previous high drive).

(ii) Hysteresis loop of a type 2 RIS film with composition 85 per cent Ni, 15 per cent Fe, thickness 800 Å, made at an evaporation rate of 31 Å/minute at a substrate temperature of 300°C (a is the major loop when peak drive field was 70 oe, b is the low-drive response in a direction parallel to that of a previous high drive, c is the low-drive response in a direction perpendicular to that of a previous high drive).

(iii) Hysteresis loop of a mottled film with composition 83 per cent Ni, 17 per cent Fe, thickness 6000 Å, made at an evaporation rate of 63 Å/minute at a substrate temperature of 300°C. Major loop when peak drive field was 210 oe.

Earlier reports[9] describe the production of RIS films (previously called "rotatable anisotropy" films) by evaporation of Permalloy on an oxide undercoating, electroplating on annealed gold films, and by annealing previously prepared films in vacuum.[10] It is thought that the previously reported[9] techniques of evaporation in an oxygen atmosphere and oxidation of previously prepared films are really examples of the production of RIS films by annealing, and are not caused by the action of oxygen. The technique of evaporation at low rates (about 30 Å/minute) on soft-glass substrates held at high temperatures (approximately 300°C) can now be added to this list.

3. High Coercive-Force and Mottled Films

In many of the methods for making RIS films given in the preceding section, variation of an appropriate experimental parameter will give either RIS, mottled, or high H_w and H_k (occasionally inverted) films. All the various types of anomalous films were not observed for all the methods used but, in general, a mild treatment by one of these procedures gives films with high H_w and H_k (some of which are inverted), a moderate treatment yields RIS films, and a drastic treatment gives mottled films. There is difficulty in obtaining reproducible results by these techniques, however, so the exact type of anomalous films that will result from a given treatment cannot always be precisely predicted.

For example, in the slow-rate high-substrate-temperature technique, H_k and H_w both rise as the substrate temperature increases until the RIS stage is reached. The same phenomenon is noted for increasing underlayer thickness in the aggregated-underlayer technique, and for electroplating on annealed gold films when the gold is more drastically annealed. The directional deviation of the easy axis (angular dispersion) was measured by the hysteresigraph method of Crowther;[11] it was found that the dispersion increased monotonically as the RIS character of the film became more pronounced. Inverted films are most often produced when the appropriate parameter is chosen to be slightly less than that which gives RIS films, but the production of inverted films is still largely unpredictable.

Thin films (less than about 1000 Å thick) show RIS properties when prepared by the technique of slow-rate high-substrate temperature (Sec. VII-A-2); thicker films (with nonpositive

magnetostriction) prepared by the same method are mottled. Similarly, films deposited on a thin undercoating of aggregated iron have RIS properties, whereas a thick undercoating (about 25 Å of Fe) yields mottled films.

4. Model for Anomalous Films and Supporting Evidence

It is proposed that the various techniques for production of anomalous films cause the formation of small, scattered inhomogeneities that have high values of magnetic anisotropy. When the film is mildly treated, the anisotropy-center density and values of the anisotropy are low, and high coercive-force films result. As the treatment becomes more drastic, the center density and value of the anisotropy rises until first RIS, then mottled, films result.

a. RIS Films

The hysteresigraph behavior of type 1 and 2 films is due to "locking" of the magnetization at the high anisotropy regions. This is seen in Bitter patterns obtained when a high AC field is applied and then removed. As discussed above, the type 2 effect is an AC one; the Bitter patterns obtained under AC conditions should thus be, and actually are, entirely different for the two types of films. When a large 60-cps field is applied in an arbitrary direction and then removed from a type 1 film, no pattern is seen because the magnetization is left parallel to the field direction. On the other hand, an intense locking pattern is observed under the same conditions for a type 2 film (Fig. VII-2). Thus the type 2 film is left in the state of magnetization illustrated by Fig. VII-3.

The behavior of the two types of film in a hysteresigraph is now clear. When a large AC field is applied to a type 1 film, the magnetization is left parallel to the field direction. The initial susceptibility is negligible in the direction of the large AC field because the magnetization cannot change until the domain walls come in. The initial susceptibility perpendicular to the large AC field is high since the magnetization is now perpendicular to the test field, and the large torque thus applied causes rotation of the magnetization. Therefore, it looks as if an easy axis were introduced parallel to the high AC field direction. The foregoing is also true for a large DC field applied to either type of film.

The conditions are reversed for hysteresigraph measurements of type 2 films. Since the magnetization state after application of a high AC field is as pictured in Fig. VII-3, it appears that a small AC test field in the direction of the high AC field (horizontal direction) will cause rotation of the magnetization in the long domains into the direction of the test field, because the torque is now large. If the test field is applied in the direction perpendicular to the high AC field direction, the magnetization configuration cannot change; the magnetization configuration is stable under these circumstances because, if the magnetization in the up- and down-directed domains were to rotate, magnetic charges would be built up on the walls to put restoring torques on the magnetization. Thus the initial susceptibility is high parallel to the high AC field direction and zero in the perpendicular direction. It thus looks as if an easy axis were produced perpendicular to the high AC field direction.

b. High Coercive-Force and Mottled Films

When the treatment of the films is mild, the anisotropy-center density is too low for the RIS property to exist; however, the anisotropy-center density is high enough to cause high values

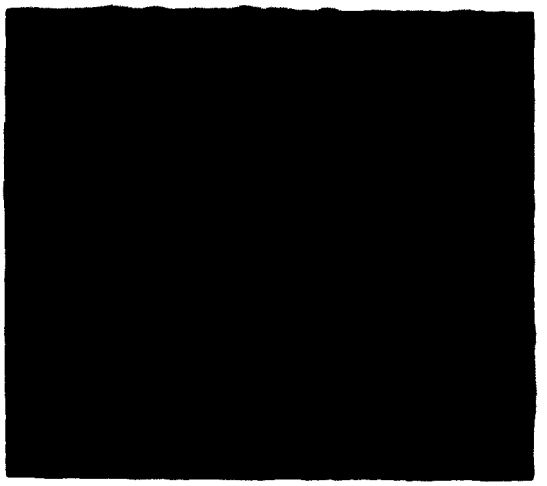

Fig. VII-2. Bitter pattern of a type 2 RIS film. A high 60-cps field was applied along the easy axis (horizontal direction) and then removed. The film composition was 83 per cent Ni, 17 per cent Fe, thickness 300 Å, made at an evaporation rate of 30 Å/minute at a substrate temperature of 300°C.

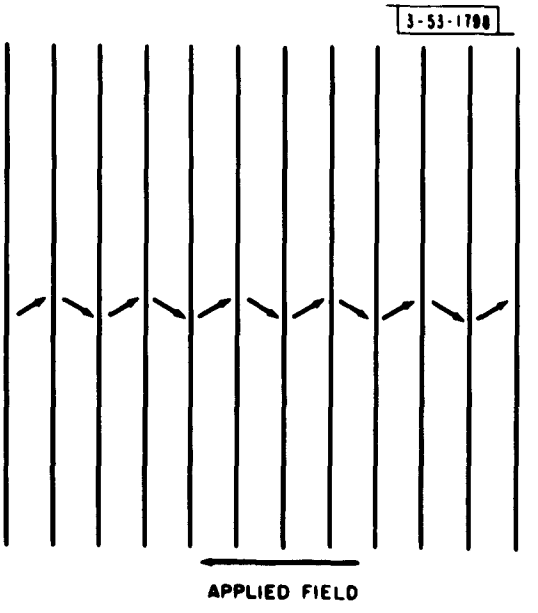

Fig. VII-3. Schematic diagram of the state of magnetization in a type 2 RIS film after application, then removal, of a large AC field. The small arrows indicate the magnetization direction.

of easy axis dispersion in the film, which results in high values of H_w and H_k. If, on the other hand, a value of the appropriate experimental parameter is chosen which is larger than that necessary for RIS films, the density and magnitude of the anisotropy centers increase and mottled films result. This high-anisotropy-center density causes a tortuous magnetization configuration which is reflected in the low remanence of the hysteresigraph loop of mottled films [Fig. VII-1(iii)] and the characteristic appearance of their Bitter patterns, which has suggested the name "mottled."

c. Origin of the Anisotropy Centers

These postulated high-anisotropy centers may conceivably be caused by crystalline anisotropy, shape anisotropy of agglomerates of crystals, antiferromagnetic exchange anisotropy caused by the presence of islands of NiO,[3,5] or inhomogeneous strain in conjunction with magnetostriction. Since anomalous films can be made by such a wide variety of techniques, it is possible that the origins of the anisotropy centers vary with the conditions of film preparation. However, there are strong indications that, at least for most of the films made during the present investigation, the predominant effect is inhomogeneous strain in conjunction with magnetostriction.

The deepest insight into this question is perhaps provided by torque-magnetometer studies. Mottled and RIS films show rotational hysteresis in their torque curves (Fig. VII-4) which disappears at high fields.[12,13] The strength of these critical fields is an indication of the value of the highest anisotropy in the anisotropy centers. For some anomalous films, the critical field is higher than that which could reasonably be caused by crystalline anisotropy. When the sample is heated in the torque magnetometer, the rotational hysteresis is found to decrease as a function of temperature, thus ruling out geometric anisotropy. In contrast to the findings of Lommel,[5] the temperatures at which the rotational hysteresis disappeared were scattered throughout the range from about 200° to 500°C for different films, thus making it unlikely that antiferromagnetic NiO plays a significant role. The following facts are in favor of the strain mechanism: (1) RIS films are more easily prepared for negative magnetostriction compositions (although they can also be prepared for positive magnetostriction compositions), whereas mottled films can be made only for negative magnetostriction compositions, and (2) stripping mottled films from the substrate (thus changing the state of strain) changes the appearance of the Bitter patterns and hysteresigraph loops. The temperature dependence of the rotational hysteresis can be interpreted as a strain-annealing effect.

M. S. Cohen

B. ISOTROPIC STRESS MEASUREMENTS IN PERMALLOY FILMS

Isotropic stress measurements in Permalloy films have been carried out as a function of thickness, rate of deposition and substrate temperature.[14] The measurements were made by clamping one end of a substrate consisting of a thin strip of glass or mica and observing the deflection of the free end during deposition. Results indicate that the stress is independent of thickness in the range 100 to 2000 Å. However, at substrate temperatures in excess of $T_a \approx 300$°C, the state of stress changes from compressive to tensile. The temperature T_a varies with the deposition rate, increasing to $T_a \approx 360$°C for rates as high as 250 Å/minute.

G. P. Weiss
D. O. Smith

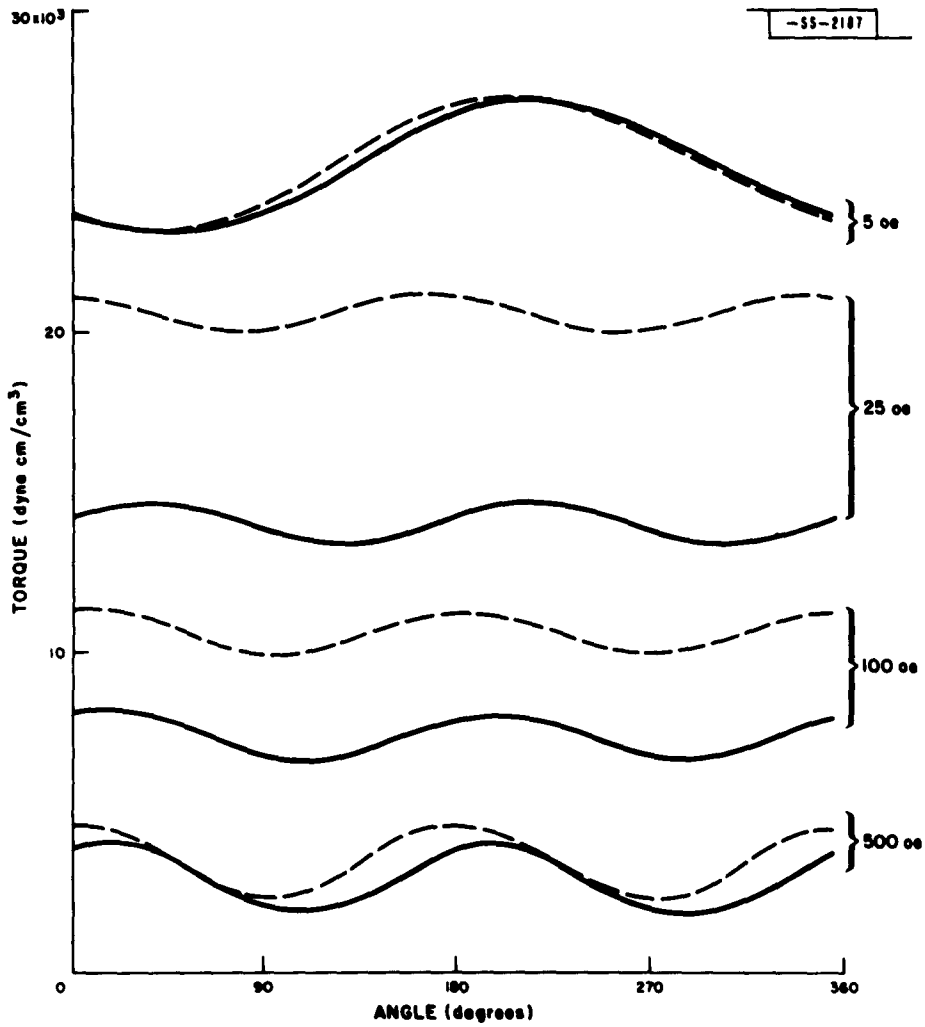

Fig. VII-4. Torque-magnetometer curves for various applied fields for a film that tends toward type 2 RIS; torque vs angle of applied field. The composition of the film was 83 per cent Ni, 17 per cent Fe, thickness 600 Å; it was deposited at a rate of 38 Å/minute at a substrate temperature of 300°C. The solid curves were taken at a clockwise and the dashed at a counterclockwise rotation of the applied field. For convenience, all curves have been plotted on the same graph; the position of the zero of torque is arbitrary.

C. DOMAIN-WALL STORAGE AND LOGIC

The operation of read-in, shifting, conditional erase and fan-out in a system of domain-wall storage and logic proposed by Smith[15] has been experimentally demonstrated.[16] The several operations were performed by controlling the current flowing through a configuration of wires placed closely under a 5 to 40 mil wide, 50 to 300 Å thick Permalloy strip, and the sequence of events was observed on the top side of the film by using the Bitter technique. The basic wiring geometry was a narrow-spaced grid of series-connected parallel wires that made an angle of 50° to 75° with the strip of film; the smaller angles were necessary for the thinner films. Conditional erase was most successful in films below 100 Å thick because, in this thickness, range walls of the same sense form double walls that require relatively large fields for erasure.

D. O. Smith
J. M. Ballantyne

REFERENCES

1. E.E. Huber, Jr. and D.O. Smith, J. Appl. Phys. 30, 267S (1959).
2. E.E. Huber, Jr., private communication.
3. R.J. Prosen, J.O. Holman and B.E. Gram, J. Appl. Phys. 32, 91S (1961).
4. T. Matcovich, E. Korostoff and A. Schmeckenbecher, J. Appl. Phys. 32, 93S (1961).
5. J.M. Lommel and C.D. Graham, Jr., J. Appl. Phys. 33 (to be published).
6. R.J. Prosen, J.O. Holman, B.E. Gram and T.J. Cebulla, J. Appl. Phys. 33 (to be published).
7. D.O. Smith, E.E. Huber, Jr., M.S. Cohen and G.P. Weiss, J. Appl. Phys. 31, 295S (1961).
8. E.C. Crittenden, A.A. Hudimac and R.I. Strough, Rev. Sci. Instr. 22, 872 (1951).
9. Quarterly Progress Report on Solid State Research [U], Lincoln Laboratory, M.I.T. (15 July 1961), p. 65, ASTIA 262282, H-331.
10. Ibid., p. 69.
11. The author thanks T. Crowther for making these measurements with his hysteresigraph technique.
12. M. Takahashi, D. Watanabe, T. Sasagawa, T. Kono and S. Ogawa, J. Phys. Soc. Japan 16, 1913 (1961).
13. G. Robinson, International Conference on Magnetism and Crystallography, Kyoto, Japan, September 1961; Symposium on the Electric and Magnetic Properties of Thin Metallic Layers, Louvain, Belgium, September 1961.
14. G.P. Weiss and D.O. Smith, J. Appl. Phys. (to be published).
15. D.O. Smith, Trans. IRE, PGEC (to be published).
16. J.M. Ballantyne, J. Appl. Phys. (to be published).

TABLE VIII-1

MEDIAN PARAMETER DATA
FOR 10 TEXAS INSTRUMENTS MESA TRANSISTORS

DC Parameters		High-Frequency Parameters	
BV_{CBO} (100 μa)	9.6 v	Low I_c (V_{CB} = 0, f_T = 1 kMcps)	0.80 ma
BV_{EBO} (100 μa)	2.7 v		
BV_{CEOO} (100 μa)	4.5 v	High I_c (V_{CB} = 0, f_T = 1 kMcps)	42 ma
h_{FE} (I_c = 1 ma, V_{CE} = 2.5 v)	36		
h_{FE} (I_c = 10 ma, V_{CE} = 2.5 v)	41	f_T (I_c = 1 ma, V_{CB} = 1 v)	1.3 kMcps
h_{FE} (I_c = 25 ma, V_{CE} = 2.5 v)	125	f_T (I_c = 20 ma, V_{CB} = 1 v)	3.0 kMcps
h_{FE} (I_c = 50 ma, V_{CE} = 2.5 v)	104	f_T (I_c = 20 ma, V_{CB} = 3 v)	3.3 kMcps
h_{FE} (I_c = 100 ma, V_{CE} = 2.5 v)	42		
V_{CE} sat (I_c = 50 ma, I_b = 10 ma)	377 mv	f_T (I_c = 50 ma, V_{CB} = 1 v)	1.5 kMcps
V_{BE} sat (I_c = 50 ma, I_b = 10 ma)	994 mv	K_s' (2 ma, corrected for C_{ob})	28 μμcoul/ma
I_{CO} (5.0 v)	0.29 μa		
I_{EO} (0.5 v)	0.05 μa	τ_s (I_e = 2 ma, I_c = 1 ma)	20 μμcoul/ma

TABLE VIII-2

CHANGE AS PERCENTAGE OF INITIAL MEDIAN VALUE OBTAINED
FROM PREVIOUS 25 SAMPLES

DC Parameters			High-Frequency Parameters		
Parameter	Increase (per cent)	Decrease (per cent)	Parameter	Increase (per cent)	Decrease (per cent)
BV_{CBO}		30	Low I_c (0 v, 1 kMcps)		40
BV_{EBO}	30				
h_{FE} (1 ma, 2.5 v)	500		High I_c (0 v, 1 kMcps)	no change	no change
h_{FE} (10 ma, 2.5 v)	100		f_T (1 ma, 1 v)	30	
h_{FE} (25 ma, 2.5 v)	300		f_T (20 ma, 1 v)	25	
h_{FE} (50 ma, 2.5 v)	175				
h_{FE} (100 ma, 2.5 v)	45		f_T (20 ma, 3 v)	20	
V_{CE} sat (50 ma, 10 ma)		20			
V_{BE} sat (50 ma, 10 ma)		10	f_T (50 ma, 1 v)		10
I_{CO} (5 v)		65	K_s' (2 ma corrected)	75	
I_{EO} (5 v)		~100	τ_s (2 ma, 1 ma)	80	

VIII. SEMICONDUCTOR COMPONENTS

A. UHF SWITCHING TRANSISTOR

An additional group of 10 state-of-the-art UHF switching transistors was received from Texas Instruments Incorporated, during the month of September. The median parameter data obtained from these units are listed in Table VIII-1. The change in the median parameter values, expressed as a percentage of the original value for the first 25 units, is given in Table VIII-2. Note the considerable improvement in DC values. The frequency performance is improved at low currents and essentially unchanged (or very slightly lower) at high currents. However, the charge storage has increased, and preliminary measurements indicate a slightly higher base resistance. The magnitude of these two problems will have to be investigated.

D.J. Eckl
P.E. Barck

B. FREQUENCY MEASUREMENTS

Frequency measurements on the mesa transistors have been made with the simplified test set described earlier.* This equipment is usable at a measuring frequency up to somewhat above 600 Mcps. Attempts to make measurements at 700 Mcps and above produce erroneous results due to line losses. However, a true 6-db/octave fall-off curve has been obtained out to 900 Mcps with the General Radio 1607A Bridge.

Values of f_T determined for these units range from 3 to 5 kMcps at 3 volts and 20 ma. The highest gain measured was 25 at 200 Mcps (corresponding to a gain-bandwidth product f_T of 5 kMcps). Most measurements have been made at lower frequencies with the test set and gain-bandwidth calculated as f_T. In actual fact, for computing circuits that will be used in the low hundreds of megacycles, f_T can be considered more as a figure of merit than as a meaningful frequency, and measurements made at a few hundred megacycles are quite realistic.

P.E. Barck

C. THE PHYSICAL BEHAVIOR OF A LINEARLY GRADED p-n "COLLECTING JUNCTION"

In a previous quarterly progress report† it was pointed out that a determination of the charge stored in a depletion-layer region of a p-n junction transistor requires a solution for the depletion-layer-region boundaries x_a and x_b and the hole-density distribution $p(x)$ within the region, all in terms of the applied voltage and/or current. In particular, that report described a solution for the depletion-layer region of a step p-n junction which uses a method introduced by Sah.‡ The resulting solution in this case, however, has been difficult to use in determining the stored charge in the junction.

---

* Quarterly Progress Reports on Solid State Research [U], Lincoln Laboratory, M.I.T. for: 15 January 1961, p. 77, ASTIA 254036, H-279; 15 April 1961, p. 69, ASTIA 257442, H-305.

† Quarterly Progress Report on Solid State Research [U], Lincoln Laboratory, M.I.T. (15 July 1961), pp. 78-81, ASTIA 262282, H-331.

‡ C.T. Sah, Proc. IRE 49, 601 (1961).

Perhaps the simplest case to treat is that of the linearly graded p-n junction. The notation, initial statement of the problem and boundary conditions in the case considered here are in accordance with the starred reference on page 61 and Fig. VIII-1, with the exception of the introduction of the following items:

(1) A normalized zero-order field term

$$f_o = \frac{+q}{kT} E^o \quad , \tag{1}$$

(2) A graded impurity distribution

$$N(x) = ax \quad , \tag{2}$$

(3) A modified field boundary condition

$$f(x) = \left[\frac{(J_c/qD_pN) - (1/N)(dN/dx)}{1 + 2p/N}\right]_{x=x_a, x_b} \tag{3a}$$

$$\approx \left[\frac{J_c}{qD_p(2p + N)}\right]_{x=x_a, x_b} \qquad \text{for } \frac{J_c}{qD_pa} \gg 1 \quad . \tag{3b}$$

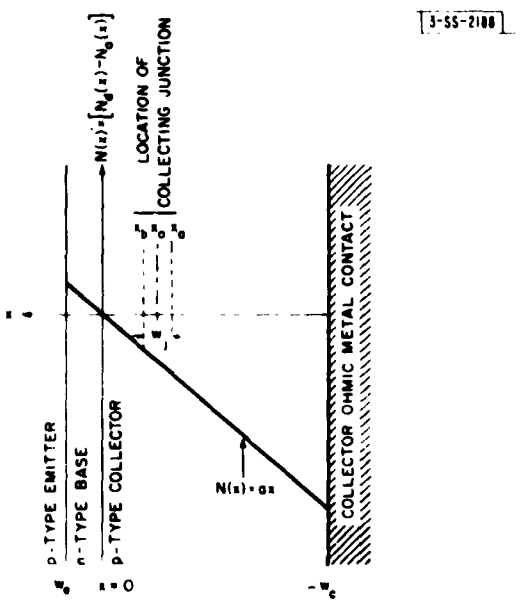

Fig. VIII-1. One-dimensional model of a linear-graded p-n-p transistor.

If the regions adjacent to the depletion layer are assumed to be approximately charge neutral, then $[p-n + N(x)]_{x=x_a, x_b} \approx 0$ and Poisson's equation for this case reduces to

$$\frac{+d^2u}{dy^2} = \frac{-q^2}{kT\epsilon f_o^2}[p-n + N] = \frac{-q^2}{kT\epsilon f_o^2}\left\{\left[(\Theta + N(x_o))\left(1 - \frac{\cosh y}{\cosh u_j}\right)\right] - \frac{a}{f}\left[y - \frac{u_j}{2}\frac{\sinh y}{\sinh(u_j/2)}\right]\right\} \quad , \tag{4}$$

where

$$y = -f_o[x - x_o] \quad \text{and} \quad \frac{u_j}{2} \geq y \geq -\frac{u_j}{2} \tag{5}$$

$$x_o = \tfrac{1}{2}(x_a + x_b) \tag{6}$$

and

$$\Theta = \left(\frac{J_p}{D_p} - \frac{J_n}{D_n}\right) \frac{1}{qf_o} \quad . \tag{7}$$

The two terms in the second line of Eq. (4) are symmetric and antisymmetric about y = 0 in the order of their appearance in the equation. The charge neutrality condition requires that

$$\int_{-u_j/2}^{u_j/2} [p-n + N]\, dy = 0 \quad . \tag{8}$$

In order that Eq. (4) satisfy Eq. (8), the symmetric term must be identically zero throughout the depletion-layer region, and thus

$$\Theta + N(x_o) = 0 \quad . \tag{9}$$

In the case of a p-n-p transistor in which the net rate of generation and recombination of hole-electron pairs within the depletion-layer regions are zero, J_p may be considered to be much greater than J_n under normal operating conditions. Thus Eq. (9) can be written in the form

$$x_o = -\frac{J_p}{qD_p a f_o} \approx -\frac{J_c}{qD_p a f_o} \quad . \tag{10}$$

For the case of the collecting junction, both the collector current density J_c and the normalized field f_o are negative values in accordance with the sign convention of Fig. VIII-1. Thus x_o is also a negative quantity, indicating that the center of the collecting junction moves into the collector p-region with increasing J_c/f_o.

The expressions for the holes and electron density distribution

$$p \approx \frac{J_p}{qD_p f_o} - \frac{1}{2}\frac{a}{f_o}\frac{u_j/2}{\sinh(u_j/2)}\, e^{-y} \tag{11}$$

$$n \approx \frac{J_n}{qD_n f_o} - \frac{1}{2}\frac{a}{f_o}\frac{u_j/2}{\sinh(u_j/2)}\, e^{y} \tag{12}$$

which result from the application of the boundary condition $[p-n + N]_{x=x_a,\, x_b} = 0$ can be used with Eq. (3) to evaluate the field boundary condition $f(x_a)$ and $f(x_b)$. At $x = x_a$, $y = u_j/2$ and $p = [n - N(x)]_{x_a} \approx -ax_a$. Thus

$$f(x_a) \approx \frac{J_c}{qD_p a x_a} \quad . \tag{13}$$

At $x = x_b$, $y = u_j/2$ and $p \approx J_p/qD_p f_o$ which in view of (10) reduces to $p \approx -ax_o$. Thus

$$f(x_b) \approx \frac{J_c}{qD_p(x_b - 2x_o)} \quad . \tag{14}$$

Since the analysis has shown that the junction is symmetrical, at least to first order, then $x_b - x_o \approx w_j/2$ and $x_a \approx x_o - w_j/2$. Thus $f(x_b)$ can be written as

$$f(x_b) = f(x_a) \approx -J_c/qD_p a x_a \quad . \tag{15}$$

The solution for x_a and x_b in terms of J_c and the normalized junction voltages u_j can now be obtained by a double integration of Poisson's equation as given by Eq. (4), after setting $\Theta + N(x_o) = 0$ and making appropriate use of the boundary conditions given by Eq. (15). This procedure yields a solution similar to Sah's of the form

$$u_j = \frac{J_c w_o}{qD_p a x_a}\left\{\frac{w_j}{w_o}\right\} + \left\{g\left(\frac{u_j}{2}\right)\right\}\left\{\frac{w_j}{w_o}\right\}^3$$

$$x_a = x_o - \frac{w_j}{2}$$

$$x_b = x_o + \frac{w_j}{2} \tag{16}$$

where

$$w_o = \left[\frac{12\epsilon kT}{q^2 a}\right]^{1/3} \tag{17}$$

and

$$\{g(u_j/2)\} = \left[1 - 3\,\frac{u_j/2\ \mathrm{ctnh}(u_j/2) - 1}{(u_j/2)^2}\right] \quad . \tag{18}$$

C. T. Kirk, Jr.

OPTICS AND INFRARED

GROUP 26

R. H. Kingston, *Leader*
F. L. McNamara, *Associate Leader*

Billups, R. R.
Bostick, H. A.
Chatterton, E. J.
O'Connor, J. R.
Rotstein, J.
Sinclair, R. S.
Underwood, D. I.
Ziegler, H. L.
Zieman, H. E.
Zimmerman, M. D.

IX. OPTICS AND INFRARED

A. SOLID STATE INFRARED IMAGE CONVERTER

The optimum operating parameters of the image converter are calculated as follows. We assume a configuration of the photoconductor and electroluminescent material as shown in Fig. IX-1 with dimensions and physical constants as shown. Now the brightness of the panel is given by (Refs. 1, 2)

$$B = B_0 \exp\left[-\left(\frac{E_0}{E}\right)^{1/2}\right] \quad ,$$

where E is the magnitude of the applied field in the electroluminescent material, and B_0 and E_0 are constants determined by the material. It should be noted that B_0 is roughly proportional to thickness and to frequency to the 0.7 power. Since we are concerned with visual or film readout of the image, we wish to optimize the contrast given by the ratio

$$\frac{\Delta B}{B} = \frac{1}{2}\left(\frac{E_0}{E}\right)^{1/2} \frac{\Delta E}{E}$$

so that the variation of B_0 does not affect the final result.

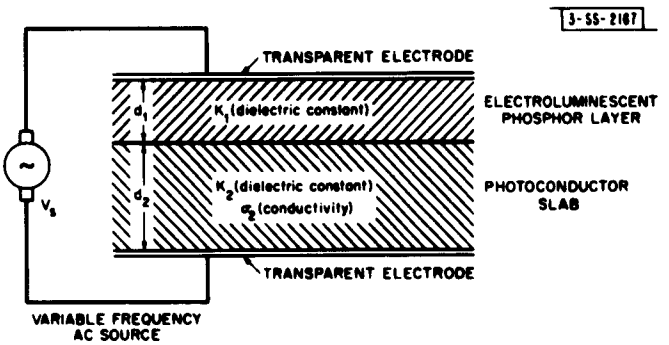

Fig. IX-1. Solid state infrared image converter.

By circuit theory it can be shown that $\Delta B/B$ is related to $\Delta\sigma/\sigma$ of the photoconductor by the relation

$$\frac{\Delta B}{B} = \frac{1}{2}\left(\frac{E_0 d_1}{V_s}\right)^{1/2} \frac{(1+2r)\,x^2}{[1+x^2(1+r)^2]^{3/4}\,[1+r^2x^2]^{5/4}} \cdot \frac{\Delta\sigma}{\sigma} \quad ,$$

where V_s is the source voltage, $r = K_2 d_1 / K_1 d_2$ and $x = \omega K_1 d_2 / \sigma d_1$.

When the driving frequency ω is adjusted so that $\omega = \sigma d_1 x_m / K_1 d_2$ where

$$x_m^2 = \frac{1+2r}{8r^2(1+r)^2}\left[1+\sqrt{1+\frac{64r^2(1+r)^2}{(1+2r)^2}}\right]$$

the contrast will be maximum and is given by

$$\frac{\Delta B}{B} = \frac{1}{2}\left(\frac{E_0 d_1}{V_s}\right)^{1/2} y(r)\,\frac{\Delta\sigma}{\sigma} \quad ,$$

where y(r), obtained by replacing x^2 by x_m^2, is a monotonically decreasing function of r, which behaves like $1/\sqrt{r}$ as r goes to zero and like $1/r$ as r goes to infinity.

Since resolution requirements and considerations of mechanical strength of the sandwich essentially fix the thickness d_2 of the photoconductor, we find that the contrast $\Delta B/B$ asymptotically approaches

$$\frac{2}{(5)^{5/4}} \left(\frac{E_o d_2}{V_s}\right)^{1/2} \left(\frac{k_1}{k_2}\right)^{1/2} \frac{\Delta\sigma}{\sigma}$$

as the thickness d_1 of the EL layer approaches zero.

Thus to obtain the largest factor multiplying the contrast sensitivity $\Delta\sigma/\sigma$ of the photoconductor, we should: (1) make the EL layer as thin as possible consistent with the light output requirements for the image converter; (2) make the source voltage as small as possible consistent with the same requirement; (3) use an EL phosphor layer that has a high dielectric constant K_1 and a large contrast factor E_0; and (4) use a photoconductor with a low dielectric constant K_2 and a thickness d_2 as large as resolution requirements permit.

M.D. Zimmerman

B. PARAMETRIC AMPLIFICATION AND OSCILLATION AT OPTICAL FREQUENCIES

Recent experimental work[3] on intense optical fields produced by a maser has indicated that it is possible to obtain variable parameter interaction in a solid. It follows that the processes of amplification and oscillation utilized in microwave devices may be extended to the optical frequency range. Specifically, we propose that coherent optical energy may be generated at subfrequencies if a nonlinear dielectric material is driven by an optical maser "pump," such as ruby. Here we derive the conditions for oscillation in a simple resonant system based on the observed experimental data for second-harmonic generation.[3-5]

Consider a resonant structure composed of two parallel highly reflecting surfaces bounding a medium of nonlinear dielectric material, such as quartz. We shall excite the medium with a traveling plane wave of frequency f_p and, by parametric excitation, produce standing waves in the medium at frequencies f_s and f_i subject to the condition that $f_p = f_s + f_i$. Here it is assumed that the thickness of the medium is such that there are resonant modes at f_s and f_i. It is also assumed that the reflectivity of the walls is small at the pump frequency so that the pump wave may propagate through the structure without appreciable reflection. Under these conditions, it may be shown that the rate of change of amplitude of the signal wave E_s due to interaction of the "idler" wave E_i with the pump is given by

$$\frac{\partial E_s}{\partial t} = \frac{1}{4\epsilon \ell} \int_o^{\ell} \exp[-jk_s z] \left(\frac{dP_s}{dt}\right) dz = \frac{j\omega_s \gamma E_i E_p}{4\epsilon \ell} \int_o^{\ell} \exp[j(k_p - k_s - k_i) z]\, dz \quad , \qquad (1)$$

where k_s, k_i and k_p are the respective wave vectors $2\pi/\lambda$ for the signal, idler and pump; and it has been assumed that the polarization of the nonlinear medium at frequency f_s is

$$P_s = \gamma_{si} E_i E_p \quad , \qquad (2)$$

where γ_{si} is a function of the three frequencies. Taking into account the "Q" of the cavity at the frequency f_s we obtain the equation

$$\frac{\partial E_s}{\partial t} = \alpha_{si} E_i - \frac{\omega_s}{2Q_s} E_s \qquad (3)$$

and a similar equation for the idler wave

$$\frac{\partial E_i}{\partial t} = \alpha_{is} E_s - \frac{\omega_i}{2Q_i} E_i \quad , \tag{4}$$

where

$$\alpha_{si} = \frac{j\omega_s \gamma_{si} E_p}{4\epsilon \ell} I_{si}(\ell) \tag{5}$$

and $I_{si}(\ell)$ is the "coherence" integral of Eq. (1). Now for oscillation, the rate of growth of the signal and idler waves should be zero or greater, and setting Eqs. (3) and (4) equal to zero yields

$$\alpha_{si}\alpha_{is} + \frac{\omega_i \omega_s}{4Q_s Q_i} = 0 \quad . \tag{6}$$

Using the "Q" of a planar cavity with power reflectivity R given by

$$Q_s = \frac{k_s \ell}{1 - R} \tag{7}$$

and setting $\omega_s \cong \omega_i \cong \omega_p/2$, we obtain

$$\frac{\omega_s^2 \gamma_{si}^2 E_p^2 I_{si}^2(\ell)}{4\epsilon^2 \ell^2} > \frac{\omega_s^2 (1 - R)^2}{k_s^2 \ell^2} \tag{8}$$

or

$$\gamma_{si}^2 E_p^2 I_{si}^2(\ell) > \frac{4\epsilon^2 \omega_s^2 (1 - R)^2}{k_s^2} \tag{9}$$

as the condition for oscillation at the frequencies f_s and f_i.

In a similar manner we may calculate the second-harmonic electric field for a traveling wave of frequency f_p, obtaining

$$E_{2p} = j\omega_p \sqrt{\mu/\epsilon} \cdot \gamma_{2p} E_p^2 \int_0^{\ell} \exp[j(2k_p - k_{2p})z]\, dz \tag{10}$$

where the polarization at frequency $2f_p$ is given by

$$P_{2p} = \gamma_{2p} E_p^2 \tag{11}$$

and the generation takes place over a path length ℓ. We now define the efficiency of second-harmonic power generation as

$$\eta = \frac{|E_{2p}|^2}{|E_p|^2} = \omega_p^2 \frac{\mu}{\epsilon} \gamma_{2p}^2 E_p^2 I_{2p}^2(\ell) \tag{12}$$

with $I_{2p}(\ell)$, the "coherence" integral of Eq. (10). For a practical experiment, with the proper choice of materials, the values of γ and the coherence integral I should be approximately the same for second-harmonic generation as for parametric mixing. Thus the inequality of Eq. (9) reduces to

$$\eta > (1 - R)^2 \tag{13}$$

for the same length ℓ and pump amplitude E_p. Recent experiments[3-5] indicate that η can be of the order of 10^{-6}, indicating that the reflectivity of the cavity walls should be 99.9 per cent or higher for oscillation. This reflectivity should be obtainable with multiple dielectric layer films. Higher pump fields which use advanced techniques should relax the above requirement.

We have considered here a special case of subfrequency generation, using a simple cavity geometry and a traveling-wave pump. There are many other possible configurations for such cavities utilizing a standing-wave pump, for example, or taking advantage of the tensor properties of the crystal to obtain longer interaction lengths, such as described in Refs. 4 and 5. It is felt that the possibility of coherent generation of lower frequencies as shown by this calculation offers great promise as an alternative source of long wavelength energy at frequencies where direct maser action is not feasible. In addition, upon the availability of continuous high-power maser sources, amplifiers may also be built by means of the above techniques. Experiments are now under way to verify the above predictions.

R. H. Kingston

REFERENCES

1. G. Destriau and H.F. Ivey, Proc. IRE 43, 1911 (1955).
2. W.A. Thornton, J. Electrochem. Soc. 107, 895 (1960).
3. P.A. Franken, et al., Phys. Rev. Letters 7, 118 (1961).
4. J.A. Giordmaine, Phys. Rev. Letters 8, 19 (1962).
5. P.D. Maker, et al., Phys. Rev. Letters 8, 21 (1962).